Journal of Sound and Vibration 509 (2021) 116246

Contents lists available at ScienceDirect

Journal of Sound and Vibration

journal homepage: www.elsevier.com/locate/jsv

Tuned nonlinear spring-inerter-damper vibration absorber for beam vibration reduction based on the exact nonlinear dynamics model

Feng Qian, Lei Zuo*

Department of Mechanical Engineering, Virginia Tech, Blacksburg, VA 24061, USA

ARTICLE INFO

Article history:
Received 8 September 2020
Revised 25 April 2021
Accepted 26 May 2021
Available online 26 May 2021

Keywords:
Inerter-damper
Vibration absorber
Energy sink
Vibration reduction
Nonlinear dynamics
Method of multiple scales

ABSTRACT

Nonlinear vibration absorbers have been extensively investigated for passive vibration control, motion isolation, and synchronous energy harvesting. This paper studies the exact nonlinear dynamics of a simply-supported beam carrying a nonlinear spring-inerter-damper energy absorber for primary resonance vibration reduction. The nonlinear governing equations of the system are derived from the energy method by considering the midplane stretching, structural discontinuity, and nonlinear boundary conditions at the spring-inerter-damper location of the beam and directly solved using the method of multiple scales. The nonlinear frequency correction factor, frequency response function, peak nonlinear frequency response, and bifurcation frequency are obtained and investigated for various system parameters. The influence of the location, spring stiffness, inertial mass, and damping of the nonlinear vibration absorber on the beam dynamics, including natural frequency, mode shape, and nonlinear frequency response, are studied. The stiffness and mass of the nonlinear vibration absorber are optimally tuned to minimize the peak nonlinear frequency response of the beam. The results show that ignoring the nonlinear boundary conditions at the spring-inerter-damper location could lead to serious underestimation of the nonlinear frequency responses. The nonlinear stiffness of the vibration absorber enhances the system nonlinearity but has no contribution to the peak nonlinear frequency response of the beam. Increasing the damping of the vibration absorber could effectively mitigate the beam vibration. When the nominal frequency of the absorber is tuned to be close to the natural frequency of the beam, the beam vibration is mostly reduced.

1. Introduction

Vibration absorbers, typically consisting of three elements, i.e., a spring, a mass, and a damper, are widely used for passive vibration control to protect engineering structures in various environments. The kinetic energy of primary structures is pumped to the subordinate vibration absorbers in the forms of the potential energy of the spring, inertial energy of the mass, and finally dissipated by the damper. Vibration absorbers are categorized into linear and nonlinear systems, which serve, in essence, as energy sinks because of their capability of transferring, absorbing, and dissipating vibration energy.

* Corresponding author.
E-mail address: leizuo@vt.edu (L. Zuo).

https://doi.org/10.1016/j.jsv.2021.116246

Nevertheless, the nonlinear vibration absorber (NVA) is substantially different from a nonlinear energy sink (NES) whose spring is essentially nonlinear, i.e., no linear stiffness component [1]. Generally, the NVA includes a nonlinear spring with both linear and nonlinear components. Therefore, it is also referred to as the variant NES [2]. Linear vibration absorbers or energy sinks are only effective at the system resonant frequency [3,4]. Consequently, significant performance degradation happens if the excitation frequency slightly deviates away from the resonant frequency. However, engineering structures are usually exposed to the ambient environment, containing multiple or random frequency components.

Nonlinear systems have been featured with broadband frequency response curves that either bend to the right or left hand depending on the types of nonlinear stiffness. The extended frequency bandwidth enables passive energy transfer from primary structures to the attached NESs over a wide range of frequencies. Therefore, it could effectively improve vibration reduction performance [5]. Jiang et al. reported that the NES is capable of absorbing steady-state vibration of a weakly coupled system over a relatively broad frequency range [6]. Mao et al. found that an optimized nonlinear torsional energy sink could restrain up to 90% vibration of the flexible primary structure [7]. Zhang et al. concluded that the ungrounded NES has a great potential for the vibration control of an axially moving beam based on the numerical study [8]. Moreover, the internal resonance, nonlinear mode interaction, and super- and subharmonics in possession of nonlinear systems allow NESs to receive and dissipate vibration energy by a series of resonance captures with highly energetic structural modes [9,10]. Recently, Chen et al. developed a magnetic bi-stable NES for seismic control of building structures and proved that the broadband internal resonance captures are essential for good performance [11]. Sigalov et al. showed that an inertially-coupled rotational NES is capable of engaging in resonance with the linear oscillator and accomplishes the targeted energy transfer over a wide frequency bandwidth [10]. As most research focuses on a single NES, Taghipour and Dardel found that the system with two NESs achieved more robust dynamics against the parameter changes of the primary structure subjected to harmonic excitations [12].

Beams carrying a vibration absorber or NES have been extensively investigated because numerous mechanical components and infrastructural structures can be modeled as beams in practice. Pakdemirli and Nayefh reported that the frequency response curves of a simply-supported beam depend on the beam midplane stretching and the parameters of the attached spring-mass system [13]. Later, Özkaya et al. extended the study by considering different beam boundary conditions and ignoring the nonlinear spring element to facilitate the analysis of the midplane stretching effect [14]. Georgiades and Vakakis showed that the NES could irreversibly absorb shock energy and achieve broadband targeted energy transfer from a flexible linear beam subjected to shock excitation [15]. Samani et al. studied the performance of NESs with monomial, polynomial, and piecewise stiffness for the control of a beam subjected to a moving load/vehicle [16]. Chtiba et al. proposed an optimal design that could confine the vibration energy of a simply-supported beam into a set of vibration absorbers and then used piezoelectric elements to harvester the confined energy [17]. A parametric analysis was conducted to find the optimal parameters that minimize the vibration amplitude. Parseh et al. compared the steady-state dynamics of a linear Euler-Bernoulli beam carrying an NES and a linear tuned mass damper (TMD) [18]. The robustness of the steady-state dynamics of the beam with the NES was also examined for different beam boundary conditions [5]. Later, Parseh et al. also studied the nonlinear damped beam coupled to the NES and found a significant reduction in the amplitude vibration [19].

Beams with joints, supports, and attachments, such as NESs, TMDs, and NVAs, are usually referred to as discontinuous beams [20]. The discontinuity could lead to significant abrupt changes in boundary conditions at the installation position of the attachment, particularly as the stiffness of the spring and the weight of the mass are comparable to these of the beam. However, most studies didn't consider the abrupt change in the boundary conditions of the discontinuous beam at the vibration absorber or NES location, and the mode shapes of the beam alone were widely used in the modeling for simplicity. Only a few works have taken into account the effect of the accessory elements (spring-mass, vibration absorber, or NES) on the boundary condition, natural frequency, and mode shapes of the primary beam [13,14,21]. However, recent research has shown that the ignorance of the effects of the changes in the boundary condition and the accessory unit could result in extreme overestimation of the vibration amplitude and detuning frequency by 80% and 1200%, respectively [21]. This impact can be even more prominent when the parameters of the vibration absorber or NES are tuned. Nevertheless, optimally tuning the parameters is substantially desirable for maximum vibration reduction. Starosvetsky and Gendelman demonstrated that a properly tuned NES could annihilate dangerous periodic regimes arising due to the nonlinearity of the system [22]. The vibration absorption characteristics of the NES can be enhanced by appropriately tuning its mass ratio and installation position on a beam [23]. The parameters of the attached NES on a nonlinear beam were optimized using both the sensitivity analysis and particle swarm optimization algorithm to achieve good efficiency of the targeted energy transfer [24].

Research has shown that a larger mass element of the NES is preferable to enhance the vibration suppression of a truss core sandwich beam for efficient nonlinear energy transfer [25]. This is mainly because a larger mass in the NES can store more inertia energy transferred from the primary structure. However, implementing the NES with a large physical mass unit can be a practical challenge since large space to accommodate the NES and the resultant long stroke is usually not available for most primary systems. Zang et al. proposed a lever-like NES by connecting the NES with the primary system through a lever to reduce the physical mass, which could substantially amplify the reaction effect of the NES [26,27]. Recently, a two-terminal mechanical device, namely, inerter, has received explosively increasing attention for passive control attributed to its distinct advantage of the mass-amplification effect. The device can be realized by rack-pinion and ball-screw mechanisms and provides an inertial force proportional to the relative acceleration between the two terminals [28]. For instance, a 300-kg apparent mass was achieved by a ball-screw device with only 2-kg physical mass [29]. Feng et al. developed a nonlinear inertia design comprising of rotational discs and leverage to improve the vibration isolation at low frequencies and/or in a broadband frequency range [30]. Javidialesaadi and Wierschem placed an inerter between the NES mass and the primary system to enhance the passive vibration control with a reduction in the RMS response by 20% ~ 25% compared to the system with a typical NES [31]. Zhang et al. demonstrated that an NES-inerter is more effective in vibration suppression than a convenient NES in terms of the energy dissipation and frequency amplitude responses [32]. Recently, Chen et al. replaced the physical mass with an inerter to reduce the weight of the attached energy absorber and achieved effective multi-mode resonance control of a composite plate over a wide frequency range [33]. Jin et al. proposed two inerter-based vibration absorbers with the elements in different configurations for minimizing the vibration response of a beam and found the inerter-based dynamic vibration absorber achieved better performance than a traditional dynamic vibration absorber for the vibration control of a simply-supported beam [34]. To the author's best knowledge, no effort has been devoted to understanding the exact nonlinear dynamics and vibration reduction of a simply-supported beam carrying a tuned inerter-based NVA by considering the abrupt changes in the boundary conditions of the beam at the NVA location. Nevertheless, it is essential to reduce the physical mass of the absorber without sacrificing vibration reduction performance, particularly for beams since modern engineering systems, such as large-span bridges, super high-risk buildings, and spacecraft have an increasing requirement to light beam-like structures.

This paper studies the exact nonlinear dynamics of a simply-supported beam carrying an inerter-based NVA (variant NES) by considering the changes in the boundary conditions of the beam-spring-inerter-damper (BSID) system. A two-terminal inerter is used to replace the physical mass element in the traditional NVA to reduce the overall weight. The inerter and damper used in this study are assumed to be created by an electromagnetic generator that converts the vibration energy into electricity and is connected to an external electrical resistor for energy dissipation. The inerter was configured in parallel with the damper to simulate the rotational electromagnetic energy harvesting device [35] which is connected to the beam through a nonlinear spring. The governing equations of the BSID system are derived by energy method and analytically solved using the method of multiple scales (MMS) to derive the analytical solutions. The natural frequencies, nonlinear correction factor, and frequency responses curves are obtained. The influence of the parameters of the NVA on the dynamic characteristics of the beam and the primary resonance vibration reduction performance is studied by analytical analysis and numerical simulations. The optimum parameters of the NES are tuned, and the analytical condition that minimizes the peak frequency response of the beam is formulated and numerically verified.

2. Theoretical modeling

The schematic diagram of the considered system is illustrated in Fig. 1(a), which consists of a simply-supported beam of length L and an attached NVA at the location of $x = x_s$. The conventional NVA comprising three elements, i.e., a mass, a nonlinear spring, and a damper, is shown in Fig. 1(b) [13,32,36,37], which could be configured in different layouts. The other end of the conventional NVA could be either free or grounded, leading to different system dynamics. A large mass is usually needed to achieve better energy absorbing performance so that the beam vibration could be effectively controlled. However, accommodating a large mass and its long motion stroke requires a large space that results in an awkward overall system. This study proposes to use a spring-inerter-damper NVA, as illustrated in Fig. 1(c), to substitute the conventional NVA with the main purpose of reducing the physical weight of the mass element. The inerter damper is a two-terminal mechanical device with an embedded rotational electromagnetic generator and flywheel that could be realized by rack-pinion or ball-screw mechanisms converting mechanical translation motion into rotation. As an example, Fig. 1(d) shows an inerter-damper based on the ball-screw mechanism initially designed for energy harvesting from railway track vibrations

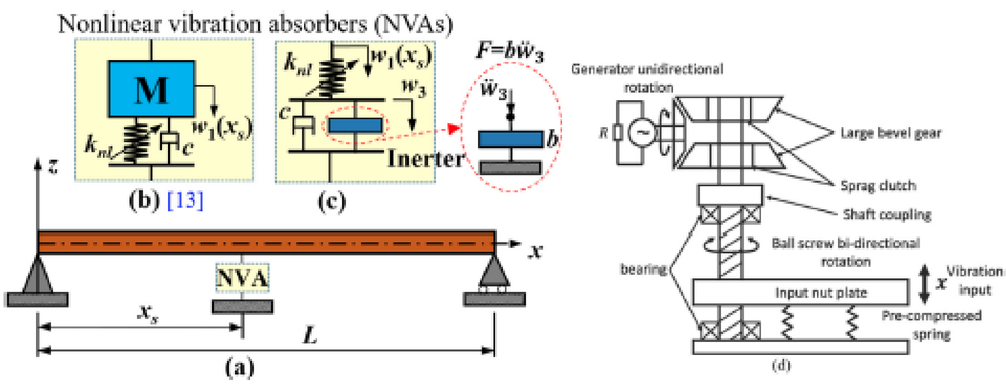

Fig. 1. The beam-spring-inerter-damper (BSID) system: (a) the overall system; (b) a typical nonlinear vibration absorber [13]; (c) proposed nonlinear spring-inerter-damper vibration absorber; (d) example of an energy harvesting inerter-damper based on the ball-screw mechanism [35].

[35]. This device provides an inertial force proportional to the relative acceleration between its two terminals and electrical damping due to the shunted external resistive load. For the proposed system, it is essential to fix the bottom end of the spring-inerter-damper to the ground to achieve the relative motion between the two terminals of the device. In addition to vibration absorption, another practical application example of the proposed system is the railway energy harvesting from train-track vibrations [35]. The train-track segment between two ballasts could be modeled as a simply-supported beam. The rotational electromagnetic energy harvester with a flywheel connected to the beam with a spring could be modeled as a nonlinear spring-inerter-damper vibration absorber.

Let ρ, E, and A denote the density, Young's modulus, and cross-sectional area of the beam, I be the moment of inertia of the beam's cross section with respect to the neutral axis, b be the inertia mass of the inerter, and k_1 and k_3 be the linear and nonlinear stiffness of the nonlinear spring. Considering the potentially abrupt changes in the boundary conditions of the beam at the NVA location ($x = x_s$), e.g., bending moment and shear forces, the beam is modeled as two segments in this study. The total kinetic and potential energy of the system can be written as

$$T = \frac{1}{2}\int_0^{x_s} \rho \dot{w}_1^2 \mathrm{d}x + \frac{1}{2}\int_{x_s}^{L} \rho \dot{w}_2^2 \mathrm{d}x + \frac{1}{2} b \dot{w}_3^2 \tag{1}$$

$$\begin{aligned} U = {} & \frac{1}{2}\int_0^{x_s} EI(w_1'')^2 \mathrm{d}x + \frac{1}{2}\int_{x_s}^{L} EI(w_2'')^2 \mathrm{d}x + \frac{1}{2}\int_0^{x_s} EA\left(u_1' + \frac{1}{2}w_1'^2\right)^2 \mathrm{d}x + \frac{1}{2}\int_{x_s}^{L} EA\left(u_2' + \frac{1}{2}w_2'^2\right)^2 \mathrm{d}x \\ & + \frac{1}{2}k_1\Big[w_1(x_s) - w_3\Big]^2 + \frac{1}{4}k_3\Big[w_1(x_s) - w_3\Big]^3 \end{aligned} \tag{2}$$

where w_1 and w_2 are the transverse displacements of the beam segments on the right and left sides of the inerter-based NVA, u_1 and u_2 are the axial displacements of the right and left beam segments, and w_3 is the linear stroke of the inerter. The prime and over dots denote the derivatives with respect to the spatial coordinate x and time t, respectively. It's worth mentioning that the axial inertial of the beam is ignored in the study because of the insignificance of the axial motion compared with the transverse motion for the simply-supported beam. Assume the damping coefficients of the right and left beam segments are c_1 and c_2, while c_3 is the damping coefficient of the inerter-damper. The virtual work done by the generalized damping forces can be written as

$$\delta W = -\int_0^{x_s} c_1 \dot{w}_1 \delta w_1 \mathrm{d}x - \int_{x_s}^{L} c_2 \dot{w}_2 \delta w_2 \mathrm{d}x - c_3 \dot{w}_3 \delta w_3 \tag{3}$$

The system is subjected to Hamilton's principle

$$\int_{t_1}^{t_2} \delta(T - U + W)\mathrm{d}t = 0 \tag{4}$$

Substituting Eqs. (1), (2), and (3) into Eq. (4) and performing the variational operation, one can obtain the governing equations and boundary conditions of the BSID system as follows.

$$EA\left(u_i' + \frac{1}{2}w_i'^2\right)' = 0, \quad i = 1, 2 \tag{5}$$

$$\rho A \ddot{w}_i + EI w_i^{iv} + c_i \dot{w}_i = EA\left[\left(u_i' + \frac{1}{2}w_i'^2\right)w_i'\right]' \tag{6}$$

$$b\ddot{w}_3 - k_1[w_1(x_s) - w_3] - k_3[w_1(x_s) - w_3]^3 + c_3\dot{w}_3 = 0 \tag{7}$$

where $i = 1, 2$ indicate the left and right beam segments. The boundary conditions at the two ends ($x = 0, L$) of the simply-supported beam and the location ($x = x_s$) of the NVA are also derived from Hamilton's principle and given by

$$w_1(0,t) = w_1''(0,t) = 0, \;\; w_2(L,t) = w_2''(L,t) = 0 \tag{8}$$

$$w_1(x_s,t) = w_2(x_s,t), w_1'(x_s,t) = w_2'(x_s,t), w_1''(x_s,t) = w_2''(x_s,t) \tag{9}$$

$$EIw_1'''(x_s,t) - EIw_2'''(x_s,t) - k_1[w_1(x_s,t) - w_3(t)] - k_3[w_1(x_s,t) - w_3(t)]^3 = 0 \tag{10}$$

$$u_1(0,t) = 0, \;\; u_2(L,t) = 0, \;\; u_1'(x_s,t) + \frac{1}{2}w_1'^2(x_s,t) - \left[u_2'(x_s,t) + \frac{1}{2}w_2'^2(x_s,t)\right] = 0 \tag{11}$$

It should be noted that the displacements in the boundary conditions (8)-(11) are written as the functions of both coordinate x and time t for clarity, which are dropped in other equations for simplicity. Integrating Eq. (5), using the boundary conditions in Eq. (11), and adding the two equations together, one has

$$u_1' + \frac{1}{2}w_1'^2 = u_2' + \frac{1}{2}w_2'^2 = \frac{1}{2L}\left[\int_0^{x_s}\frac{1}{2}w_1'^2\mathrm{d}x + \int_{x_s}^{L}\frac{1}{2}w_2'^2\mathrm{d}x\right] \tag{12}$$

Substituting Eqs. (5) and (12) into Eq. (6), the governing Eq. (6) can be rewritten as

$$\rho A\ddot{w}_1 + EIw_1^{iv} + c_1\dot{w}_1 = \frac{EA}{2L}\left(\int_0^{x_s}\frac{1}{2}w_1'^2\mathrm{d}x + \int_{x_s}^{L}\frac{1}{2}w_2'^2\mathrm{d}x\right)w_1'' \tag{13}$$

$$\rho A\ddot{w}_2 + EIw_2^{iv} + c_2\dot{w}_2 = \frac{EA}{2L}\left(\int_0^{x_s}\frac{1}{2}w_1'^2\mathrm{d}x + \int_{x_s}^{L}\frac{1}{2}w_2'^2\mathrm{d}x\right)w_2'' \tag{14}$$

It's worth mentioning that the terms in the right-hand side of Eqs. (13) and (14) are induced by the axial motions of the beam, which are referred to as the stretching of the midplane [13], the following dimensionless quantities are introduced to nondimensionalize the system,

$$\bar{x} = \frac{x}{L},\ \bar{w}_i = \frac{w_i}{L},\ \eta = \frac{x_s}{L},\ \bar{t} = \frac{t}{L^2}\sqrt{\frac{EI}{\rho A}},\ \mu = \frac{b}{\rho AL} \tag{15}$$

where the parameter μ is termed as the mass ratio of the inerter to the total mass of the beam. Substituting the dimensionless quantities into the governing Eqs. (7), (13)-(14), one has

$$\ddot{\overline{w}}_1 + 2\overline{\zeta}_1\dot{\overline{w}}_1 + \overline{w}_1^{iv} = \lambda\left(\int_0^{\eta}\frac{1}{2}\overline{w}_1'^2\mathrm{d}\overline{x} + \int_{\eta}^{1}\frac{1}{2}\overline{w}_2'^2\mathrm{d}\overline{x}\right)\overline{w}_1'' \tag{16}$$

$$\ddot{\overline{w}}_2 + 2\overline{\zeta}_2\dot{\overline{w}}_2 + \overline{w}_2^{iv} = \lambda\left(\int_0^{\eta}\frac{1}{2}\overline{w}_1'^2\mathrm{d}\overline{x} + \int_{\eta}^{1}\frac{1}{2}\overline{w}_2'^2\mathrm{d}\overline{x}\right)\overline{w}_2'' \tag{17}$$

$$\mu\ddot{\overline{w}}_3 + 2\overline{\zeta}_3\dot{\overline{w}}_3 - \kappa_1[\overline{w}_1(\eta,t) - \overline{w}_3] - \kappa_3[\overline{w}_1(\eta,t) - \overline{w}_3]^3 = 0 \tag{18}$$

where $\overline{\zeta}_1 = \frac{c_1L^2}{2EI}\sqrt{\frac{EI}{\rho A}}$, $\overline{\zeta}_2 = \frac{c_2L^2}{2EI}\sqrt{\frac{EI}{\rho A}}$, and $\overline{\zeta}_3 = \frac{c_3L}{2EI}\sqrt{\frac{EI}{\rho A}}$ are dimensionless damping ratios, $\lambda = \frac{AL}{2I}$, $\kappa_1 = \frac{k_1L^3}{EI}$ and $\kappa_3 = \frac{k_3L^5}{EI}$ are dimensionless linear and nonlinear stiffness of the nonlinear spring. Substituting the dimensionless quantities into the boundary conditions (8)-(11), one has

$$\overline{w}_1(0,\bar{t}) = \overline{w}_1''(0,\bar{t}) = 0,\ \overline{w}_2(0,\bar{t}) = \overline{w}_2''(0,\bar{t}) = 0 \tag{19}$$

$$\overline{w}_1(\eta,\bar{t}) = \overline{w}_2(\eta,\bar{t}),\ \overline{w}_1'(\eta,\bar{t}) = \overline{w}_2'(\eta,\bar{t}),\ \overline{w}_1''(\eta,\bar{t}) = \overline{w}_2''(\eta,\bar{t}) \tag{20}$$

$$\overline{w}_1'''(\eta,\bar{t}) - \overline{w}_2'''(\eta,\bar{t}) - \kappa_1[\overline{w}_1(\eta,\bar{t}) - \overline{w}_3(\bar{t})] - \kappa_3[\overline{w}_1(\eta,\bar{t}) - \overline{w}_3(\bar{t})]^3 = 0 \tag{21}$$

Adding forcing terms to the governing Eqs. (16) and (17) and dropping the over hat for simplicity from all the displacement and time variables, one has

$$\ddot{w}_1 + 2\overline{\zeta}_1\dot{w}_1 + w_1^{iv} = \lambda\left(\int_0^{\eta}\frac{1}{2}w_1'^2\mathrm{d}x + \int_{\eta}^{1}\frac{1}{2}w_2'^2\mathrm{d}x\right)w_1'' + \overline{F}_1\cos\Omega t \tag{22}$$

$$\ddot{w}_2 + 2\overline{\zeta}_2\dot{w}_2 + w_2^{iv} = \lambda\left(\int_0^{\eta}\frac{1}{2}w_1'^2\mathrm{d}x + \int_{\eta}^{1}\frac{1}{2}w_2'^2\mathrm{d}x\right)w_2'' + \overline{F}_2\cos\Omega t \tag{23}$$

$$\mu\ddot{w}_3 + 2\overline{\zeta}_3\dot{w}_3 - \kappa_1[w_1(\eta,t) - w_3] - \kappa_3[w_1(\eta,t) - w_3]^3 = 0 \tag{24}$$

$$w_1(0,t) = w_1''(0,t) = 0,\ w_2(L,t) = w_2''(L,t) = 0 \tag{25}$$

$$w_1(\eta,t) = w_2(\eta,t),\ w_1'(\eta,t) = w_2'(\eta,t),\ w_1''(\eta,t) = w_2''(\eta,t) \tag{26}$$

$$w_1'''(\eta,t) - w_2'''(\eta,t) - \kappa_1[w_1(\eta,t) - w_3(t)] - \kappa_3[w_1(\eta,t) - w_3(t)]^3 = 0 \tag{27}$$

where $\overline{F}_1$ and $\overline{F}_2$ are the excitation amplitude and Ω is the excitation frequency.

3. Multiple scales solutions

Since the purpose of this study is to investigate the primary resonance vibration reduction of the beam, only the primary resonance response is considered, and the method of multiple scales [38] is employed to derive the approximate analytical solution of the frequency response. The damping and forcing terms in the governing equations are ordered as small terms, i.e., $\overline{\zeta}_i = \varepsilon^2\zeta_i$ and $\overline{F}_i = \varepsilon^3 F_i$, $i = 1, 2$, so that these terms counter the effect of the weakly nonlinear terms. To apply the method of multiple scales, the solutions of the displacements are expanded in the fast and low time scales of $T_0 = t$ and $T_2 = \varepsilon^2 t$ as follows

$$w_1(x,t) = \varepsilon w_{11}(x, T_0, T_2) + \varepsilon^3 w_{13}(x, T_0, T_2) \tag{28}$$

$$w_2(x,t) = \varepsilon w_{21}(x, T_0, T_2) + \varepsilon^3 w_{23}(x, T_0, T_2) \tag{29}$$

$$w_3(t) = \varepsilon w_{31}(T_0, T_2) + \varepsilon^3 w_{33}(T_0, T_2) \tag{30}$$

The time derivatives of the solutions with respect to the multiple scale time can be obtained based on the chain rule by

$$(') = \mathrm{D}_0 + \varepsilon^2\mathrm{D}_2 + \cdots, \quad ('') = \mathrm{D}_0^2 + 2\varepsilon^2\mathrm{D}_0\mathrm{D}_2 + \cdots \tag{31}$$

where $\mathrm{D}_n = \partial/\partial \mathrm{T}_n$. Substituting Eqs. (28)-(31) into the governing equations of motion in Eqs. (22)-(24) and the boundary conditions in Eqs. (25)-(27), and equating the coefficients of the like order of ε, one can obtain the linear and nonlinear governing equations and boundary conditions for the first and third order of ε as follows

Order ε :

$$\mathrm{D}_0^2 w_{11} + w_{11}^{iv} = 0 \tag{32}$$

$$\mathrm{D}_0^2 w_{21} + w_{21}^{iv} = 0 \tag{33}$$

$$\mu\mathrm{D}_0^2 w_{31} - \kappa_1[w_{11} - w_{31}] = 0 \tag{34}$$

$$w_{11}(0, T_0) = w_{11}''(0, T_0) = 0, \; w_{21}(1, T_0) = w_{21}''(1, T_0) = 0 \tag{35}$$

$$w_{11}(\eta, T_0) = w_{21}(\eta, T_0), \; w_{11}'(\eta, T_0) = w_{21}'(\eta, T_0), \; w_{11}''(\eta, T_0) = w_{21}''(\eta, T_0) \tag{36}$$

$$w_{11}'''(\eta, T_0) - w_{21}'''(\eta, T_0) - \kappa_1[w_{11}(\eta, T_0) - w_{31}(T_0)] = 0 \tag{37}$$

Order ε^3 :

$$\mathrm{D}_0^2 w_{13} + w_{13}^{iv} = -2\mathrm{D}_0\mathrm{D}_2 w_{11} - 2\zeta_1\mathrm{D}_0 w_{11} + \frac{\lambda}{2}\left[\int_0^{\eta} w_{11}'^2 dx + \int_{\eta}^{1} w_{21}'^2 dx\right] w_{11}'' + F_1\cos\Omega t \tag{38}$$

$$\mathrm{D}_0^2 w_{23} + w_{23}^{iv} = -2\mathrm{D}_0\mathrm{D}_2 w_{21} - 2\zeta_2\mathrm{D}_0 w_{21} + \frac{\lambda}{2}\left[\int_0^{\eta} w_{11}'^2 dx + \int_{\eta}^{1} w_{21}'^2 dx\right] w_{21}'' + F_2\cos\Omega t \tag{39}$$

$$\begin{aligned}\mu\mathrm{D}_0^2 w_{33} + \kappa_1 w_{33} = &-2\mu\mathrm{D}_0\mathrm{D}_2 w_{31} - 2\zeta_3\mathrm{D}_0 w_{31} - \kappa_1 w_{13}(\eta, t) \\ &+ \kappa_3\left[w_{11}^2(\eta, t) - 3w_{11}^2(\eta, t)w_{31} - 3w_{11}(\eta, t)w_{31}^2 - w_{31}^3\right]\end{aligned} \tag{40}$$

$$w_{13}(0, T_0) = w_{13}''(0, T_0) = 0, \; w_{23}(1, T_0) = w_{23}''(1, T_0) = 0 \tag{41}$$

$$w_{13}(\eta, T_0) = w_{23}(\eta, T_0), \; w_{13}'(\eta, T_0) = w_{23}'(\eta, T_0), \; w_{13}''(\eta, T_0) = w_{23}''(\eta, T_0) \tag{42}$$

$$\begin{aligned}&w_{13}'''(\eta, T_0) - w_{23}'''(\eta, T_0) - \kappa_1[w_{13}(\eta, T_0) - w_{33}(T_0)] \\ &- \kappa_3\left[w_{11}^3(\eta, T_0) - 3w_{11}^2(\eta, T_0)w_{31}(T_0) - 3w_{11}(\eta, T_0)w_{31}^2(T_0) - w_{31}^3(T_0)\right] = 0\end{aligned} \tag{43}$$

3.1. Linear analysis

The Eqs. (32)-(34) at the order of ε are second order linear differential equations and Eqs. (35)-(37) are the associated linear boundary conditions. Using the separation of variables, the solutions are assumed to have the following forms

$$w_{11}(x, T_0, T_2) = \left[A(T_2)e^{i\omega T_0} + cc.\right]Y_1(x) \tag{44}$$

$$w_{21}(x, T_0, T_2) = \left[A(T_2)e^{i\omega T_0} + cc.\right]Y_2(x) \tag{45}$$

$$w_{31}(T_0, T_2) = \left[A(T_2)e^{i\omega T_0} + cc.\right]Y_3 \tag{46}$$

where ω is the primary resonant frequency of the system, $Y_i(x)$ are the mode shape functions, A is the complex amplitude of the response, and $cc.$ denotes the complex conjugate of the preceding terms. Substituting the solutions in Eqs. (44)-(46) into the linear governing Eqs. (32)-(34) and the linear boundary conditions in Eqs. (35)-(37), one has

$$Y_1^{iv} - \omega^2 Y_1 = 0 \tag{47}$$

$$Y_2^{iv} - \omega^2 Y_2 = 0 \tag{48}$$

$$Y_3 = Y_1(\eta)\Psi \tag{49}$$

$$Y_1(0) = Y_1''(0) = 0,\ \ Y_2(1) = Y_2''(1) = 0 \tag{50}$$

$$Y_1(\eta) = Y_2(\eta),\ \ Y_1'(\eta) = Y_2'(\eta),\ \ Y_1''(\eta) = Y_2''(\eta) \tag{51}$$

$$Y_1'''(\eta) - Y_2'''(\eta) - \kappa_1 Y_1(\eta)(1-\Psi) = 0 \tag{52}$$

where $\Psi = \frac{\kappa_1}{\kappa_1 - \mu\omega^2}$, and Eq. (49) has been substituted into the boundary condition to obtain Eq. (52). Eq. (49) shows that Y_3 characterizing the motion pattern of the inerter is a function of the beam mode shape at the installation location, linear stiffness of the NVA, mass ratio, and the natural frequency of the system.

The solutions to Eqs. (47) and (48) are the mode shapes of the two beam segments, which have exactly analytical forms as follows

$$Y_1(x) = c_{11}\sin\beta x + c_{12}\cos\beta x + c_{13}\sinh\beta x + c_{14}\cosh\beta x \tag{53}$$

$$Y_2(x) = c_{21}\sin\beta x + c_{22}\cos\beta x + c_{23}\sinh\beta x + c_{24}\cosh\beta x \tag{54}$$

where $\beta = \sqrt{\omega}$, c_{ij} ($i = 1, 2$ and $j = 1, 2, 3, 4$) are the constant coefficients to be determined by the linear boundary conditions. Substituting the mode shapes into the linear boundary conditions in Eqs. (50) and (51), one can obtain

$$Y_1(x) = \bar{c}[\tanh\beta\cos\beta\eta(\tan\beta\eta - \tan\beta)\sin\beta x - \tan\beta\cosh\beta\eta(\tanh\beta\eta - \tanh\beta)\sinh\beta x] \tag{55}$$

$$Y_2(x) = \bar{c}[\tanh\beta\sin\beta\eta(\sin\beta x - \tan\beta\cos\beta x) - \tan\beta\sinh\beta\eta(\sinh\beta x - \tanh\beta\cosh\beta x)] \tag{56}$$

where $\bar{c}$ could be determined from the orthogonal condition of mode shapes using Eqs. (47) ~ (52) and is given by

$$\bar{c}_r = \frac{1}{\sqrt{\mu\left(\bar{Y}_{1r}(\eta)\Psi_r\right)^2 + \left(\int_0^\eta \bar{Y}_{1r}^2 dx + \int_\eta^1 \bar{Y}_{2r}^2 dx\right)}} = \frac{1}{\sqrt{\mu\bar{Y}_{3r}^2 + \left(\int_0^\eta \bar{Y}_{1r}^2 dx + \int_\eta^1 \bar{Y}_{2r}^2 dx\right)}} \tag{57}$$

where r is the number of linear vibration modes, $\bar{Y}_{3r} = \bar{Y}_{1r}(\eta)\Psi_r$ in terms of Eq. (49),$\Psi_r = \frac{\kappa_1}{\kappa_1 - \mu\omega_r^2}$, and

$$\bar{Y}_{1r}(x) = \tanh\beta_r\cos\beta_r\eta(\tan\beta_r\eta - \tan\beta_r)\sin\beta_r x - \tan\beta_r\cosh\beta_r\eta(\tanh\beta_r\eta - \tanh\beta_r)\sinh\beta_r x \tag{58}$$

$$\bar{Y}_{2r}(x) = \tanh\beta_r\sin\beta_r\eta(\sin\beta_r x - \tan\beta_r\cos\beta_r x) - \tan\beta_r\sinh\beta_r\eta(\sinh\beta_r x - \tanh\beta_r\cosh\beta_r x) \tag{59}$$

It is observed that the coefficient ζ_r includes the contributions of the mode shapes of both the beam and the NVA. As the linear stiffness $\kappa_1 = 0$, it will degenerate to $\bar{\zeta}_r = \frac{1}{\sqrt{(\int_0^\eta Y_{1r}^2 dx + \int_\eta^1 Y_{2r}^2 dx)}}$, which is the modal normalization coefficient of the segmented beam only. Substituting Eqs. (55) and (56) into the boundary condition (52), the transcendental equation can be obtained as the following after some mathematical manipulation.

$$\begin{aligned}
&\left[\beta^3 \tanh\beta \cos^2\beta\eta + \kappa_1\left(1 - \frac{\kappa_1}{\kappa_1 - \mu\beta^4}\right)\tanh\beta \sin\beta\eta \cos\beta\eta\right](\tan\beta\eta - \tan\beta)\\
&+ \left[\beta^3 \tan\beta \cosh^2\beta\eta - \kappa_1\left(1 - \frac{\kappa_1}{\kappa_1 - \mu\beta^4}\right)\tan\beta \sinh\beta\eta \cosh\beta\eta\right](\tanh\beta\eta - \tanh\beta)\\
&+ \beta^3\Big[\tanh\beta \sin\beta\eta(-\tan\beta \sin\beta\eta - \cos\beta\eta) - \tan\beta \sin\beta\eta(\cosh\beta\eta - \tanh\beta \sinh\beta\eta)\Big] = 0
\end{aligned} \tag{60}$$

Solving the transcendental equation using numerical methods yields the values of β and the natural frequencies of the beam-spring-inerter-damper system. It can be seen that both the mode shapes in Eqs. (55)-(56) and the transcendental Eq. (60) are quite complex due to the involvement of the spring-inerter-damper NVA and the consideration of the changes in the boundary conditions of the beam at the NVA location. The dependence of the natural frequencies and mode shapes on the linear spring stiffness, inertia mass, and location of the NVA is characterized by the parameters κ_1, μ, and η in Eqs. (55)-(60). The influence of these parameters on the mode shapes and natural frequencies will be discussed later based on the simulation results.

3.2. Nonlinear analysis

The nonlinear governing Eqs. (38)-(40) have a solution only if a solvability condition is satisfied [13,14]. The solutions of the nonlinear governing equations usually comprise two parts. One part contributes to the secular terms associated with $e^{i\omega T_0}$ that finally gives the solvability condition, while the other one leads to the higher-order harmonic terms that contribute to the non-homogeneous solution. Based on the method of multiple scales, the goal here is to find the nonlinear frequency response function from the solvability condition by eliminating the secular terms. Therefore, the solutions are assumed to consist of secular and nonsecular terms to find the solvability condition, which are written as

$$w_{13}(x, T_0, T_2) = \phi_1(x, T_2)e^{i\omega T_0} + cc. + W_1(x, T_0, T_2) \tag{61}$$

$$w_{23}(x, T_0, T_2) = \phi_2(x, T_2)e^{i\omega T_0} + cc. + W_2(x, T_0, T_2) \tag{62}$$

$$w_{33}(T_0, T_2) = \phi_3(T_2)e^{i\omega T_0} + cc. + W_3(T_0, T_2) \tag{63}$$

where ϕ_i are the parts contributing to the secular terms while W_i are unique and free of secular. It is worth mentioning that the function ϕ_i substantially takes partial nonlinear mode shapes into account. In other words, the contributions of the nonlinear mode shapes to the secular terms are assumed to be ϕ_i. Since this study only considers the primary resonance response, the excitation frequency is assumed to be near to one of the natural frequencies, which could be written by

$$\Omega = \omega + \varepsilon^2\sigma \tag{64}$$

where σ is a detuning parameter. Substituting the solutions in Eqs. (61)-(63) together with Eqs. (44)-(46) into the nonlinear governing Eqs. (38)-(40) and equating the coefficients of the secular terms associated with $e^{i\omega T_0}$ on both sides of each equation, one could obtain

$$\phi_1^{iv} - \omega^2\phi_1 = -2i\omega(A' + \eta_1 A)Y_1 + \frac{3}{2}\lambda A^2\bar{A}\left(\int_0^\eta Y_1'^2 dx + \int_\eta^1 Y_2'^2 dx\right)Y_1'' + \frac{F_1}{2}e^{i\sigma T_2} \tag{65}$$

$$\phi_2^{iv} - \omega^2\phi_2 = -2i\omega(A' + \eta_2 A)Y_2 + \frac{3}{2}\lambda A^2\bar{A}\left(\int_0^\eta Y_1'^2 dx + \int_\eta^1 Y_2'^2 dx\right)Y_2'' + \frac{F_2}{2}e^{i\sigma T_2} \tag{66}$$

$$(\kappa_1 - \mu\omega^2)\phi_3 = -2\mu i\omega(A' + \zeta_3 A)Y_3 + \kappa_1\phi_1(\eta) + 3\kappa_3 A^2\bar{A}[Y_1(\eta) - Y_3]^3 \tag{67}$$

Substituting the solutions in Eqs. (61)-(63) together with Eqs. (44)-(46) into the nonlinear boundary conditions in Eqs. (41)-(43) yields

$$\phi_1(0, T_2) = \phi_1''(0, T_2) = 0, \;\; \phi_2(1, T_2) = \phi_2''(1, T_2) = 0 \tag{68}$$

$$\phi_1(\eta, T_2) = \phi_2(\eta, T_2), \;\; \phi_1'(\eta, T_2) = \phi_2'(\eta, T_2), \;\; \phi_1''(\eta, T_2) = \phi_2''(\eta, T_2) \tag{69}$$

$$\phi_1'''(\eta, T_2) - \phi_2'''(\eta, T_2) = \phi_1(\eta)\kappa_1(1-\Psi) + 2\mu i\omega(A' + \zeta_3 A)\Psi^2 Y_1(\eta) + 3\kappa_3 A^2\bar{A}Y_1^3(\eta)(1-\Psi)^4 \tag{70}$$

where Eqs. (49) and (67) have been used in deriving Eq. (70). Integrating Eq. (65)$\times Y_1$ from 0 to η and Eq. (66)$\times Y_2$ from η to 1, the following equation is derived by combining the resultant equations and considering the boundary conditions in Eqs. (50)-(52) and (68)-(69).

$$\begin{aligned}[\phi_1''' - \phi_2''']Y_1(\eta) = {} & \phi_1(\eta)Y_1(\eta)\kappa_1(1-\Psi) - 2i\omega(A' + \zeta_1 A)\Big(\int_0^\eta Y_1^2 dx + \int_\eta^1 Y_2^2 dx\Big) \\ & + \frac{3}{2}\lambda A^2\bar{A}\Big(\int_0^\eta Y_1'^2 dx + \int_\eta^1 Y_2'^2 dx\Big)\Big(\int_0^\eta Y_1'' Y_1 dx + \int_\eta^1 Y_2'' Y_2 dx\Big) \\ & + \frac{e^{i\sigma T_2}}{2}\Big(\int_0^\eta F_1 Y_1 dx + \int_\eta^1 F_2 Y_2 dx\Big)\end{aligned} \tag{71}$$

where the damping coefficients of the two beam segments are assumed to be identical, i.e. $\zeta_1 = \zeta_2$, and the derivatives of the mode shapes, i.e. $Y_1''''(x) = \omega^2 Y_1(x)$, $Y_2''''(x) = \omega^2 Y_2(x)$, have bee used to derive Eq. (71). Combining (70)$\times Y_1(\eta)$ with Eq. (71) yields the solvability condition of the nonlinear problem which is given by

$$3A^2\bar{A}\Big[\kappa_3 Y_1^4(\eta)(1-\Psi)^4 - \frac{1}{\lambda}b_2 b_3\Big] = -2i\omega(A' + \zeta_1 A)b_1 - 2i\omega\mu(A' + \zeta_3 A)\Psi^2 Y_1^2(\eta) + \frac{1}{2}b_4 e^{i\sigma T_2} \tag{72}$$

where the coefficients b_1, b_2, b_3, and b_4 are defined by

$$\begin{aligned}& b_1 = \int_0^\eta Y_1^2 dx + \int_\eta^1 Y_2^2 dx, \quad b_2 = \int_0^\eta Y_1'^2 dx + \int_\eta^1 Y_2'^2 dx, \quad b_3 = \int_0^\eta Y_1'' Y_1 dx + \int_\eta^1 Y_2'' Y_2 dx, \\ & b_4 = \int_0^\eta F_1 Y_1 dx + \int_\eta^1 F_2 Y_2 dx\end{aligned} \tag{73}$$

Integrating the expressions in b_3 by parts yields $b_3 = -b_2$. The steps went through above to derive Eq. (72) is substantially a process of canceling the unknown functions ϕ_i including partial nonlinear mode shapes, as well as their derivatives, by use of the nonlinear governing equations and boundary conditions. The first term on the left-hand side and the second term on the right-hand side of the solvability condition Eq. (72) are from the nonlinear boundary condition in Eq. (70). The second term on the left-hand side is due to the inclusion of the midplane stretching effect of the beam (b_2 and b_3).

Expanding the complex amplitude A into the polar form as

$$A = \frac{1}{2}a(T_2)e^{i\theta(T_2)} \tag{74}$$

where a and θ are the real amplitude and phase angle of the solution. Substituting Eq. (74) into the solvability condition in Eq. (72) and separating the real and imaginary parts, one can obtain the modulation equations of the amplitude and phase responses as

$$\omega b_5 a' = -\Big(b_1\zeta_1 + \mu\zeta_3\Psi^2 Y_1^2(\eta)\Big)\omega a + \frac{1}{2}b_4 \sin\gamma \tag{75}$$

$$\omega b_5 a\gamma' = \omega b_5 a\sigma - \frac{3}{8}a^3\Big[\kappa_3 Y_1^4(\eta)(1-\Psi)^4 - \frac{1}{2}\lambda b_2 b_3\Big] + \frac{1}{2}b_4\cos\gamma \tag{76}$$

where $b_5 = b_1 + \mu\Psi^2 Y_1^2(\eta)$, $\gamma = \sigma T_2 - \theta$, and $\gamma' = \sigma - \theta'$. It is noted that the second term $\mu\Psi^2 Y_1^2(\eta)$ in the coefficient b_5 is originated from the nonlinear boundary condition in Eq. (70). In order to calculate the nonlinear frequencies, the damping, excitation, and detuning parameter in Eqs. (75) and (76) are set to zero, which leads to

$$a' = 0, \text{ and thus } a = \text{constant} \tag{77}$$

$$\theta' = -\gamma' = \frac{3a^2}{8\omega b_5}\Big[\kappa_3 Y_1^4(\eta)(1-\Psi)^4 - \frac{1}{2}\lambda b_2 b_3\Big] = \vartheta a^2 \tag{78}$$

where $\vartheta = \frac{3}{8\omega b_5}[\kappa_3 Y_1^4(\eta)(1-\Psi)^4 - \frac{1}{2}\lambda b_2 b_3]$ is referred to as the nonlinear frequency correction factor [14]. It can be seen that the nonlinear frequency correction factor is induced by the nonlinear spring stiffness κ_3 of the NVA and the midplane stretching b_2 and b_3 of the beam. The nonlinear frequency is thus given by

$$\omega_{nl} = \omega + \vartheta a^2 \tag{79}$$

The steady-state periodic solutions can be numerically solved from the nonlinear frequency response function, which could be derived from Eqs. (75) and (76) by setting $a' = \gamma' = 0$ and eliminating the trigonometric functions. The nonlinear frequency response function is

$$\Big\{-\omega b_5 a\sigma + \frac{3}{8}a^3\Big[\kappa_3 Y_1^4(\eta)(1-\Psi)^4 - \frac{1}{2}\lambda b_2 b_3\Big]\Big\}^2 + \Big\{\Big[b_1\zeta_1 + \mu\zeta_3\Psi^2 Y_1^2(\eta)\Big]\omega a\Big\}^2 = \Big(\frac{b_4}{4}\Big)^2 \tag{80}$$

And the phase angle is given by

$$\gamma = \arctan \frac{[b_1\zeta_1 + \mu\zeta_3\Psi^2\Upsilon_1^2(\eta)]\omega a}{-\omega b_5 a\sigma + \frac{3}{8}a^3\left[\kappa_3\Upsilon_1^4(\eta)(1-\Psi)^4 - \frac{1}{2}\lambda b_2 b_3\right]} \tag{81}$$

Eq. (80) is a sixth-order nonlinear equation, from which multiple solutions of the real amplitude a can be numerically solved with the given frequency and detuning parameter. The stability of the solutions can be determined from the eigenvalues of the Jaccobian matrix in Eq. (82), which is obtained from Eqs. (75) and (76).

$$J = \begin{bmatrix} \frac{\partial a'}{\partial a} & \frac{\partial a'}{\partial \gamma} \\ \frac{\partial \gamma'}{\partial a} & \frac{\partial \gamma'}{\partial \gamma} \end{bmatrix} = \begin{bmatrix} -\frac{1}{b_5}\left(b_1\zeta_1 + \mu\zeta_3\Psi^2\Upsilon_1^2(\eta)\right) & -\sigma a + \frac{3a^3}{8\omega b_5}\left[\kappa_3\Upsilon_1^4(\eta)(1-\Psi)^4 - \frac{1}{2}\lambda b_2 b_3\right] \\ \frac{\sigma}{a} - \frac{9a}{8\omega b_5}\left[\kappa_3\Upsilon_1^4(\eta)(1-\Psi)^4 - \frac{1}{2}\lambda b_2 b_3\right] & -\frac{1}{b_5}\left(b_1\zeta_1 + \mu\zeta_3\Psi^2\Upsilon_1^2(\eta)\right) \end{bmatrix} \tag{82}$$

The detuning parameter σ can be solved as the function of the amplitude a and frequency ω from Eq. (80), which is

$$\sigma = \frac{3a^2}{8\omega b_5}\left[\kappa_3\Upsilon_1^4(\eta)(1-\Psi)^4 - \frac{1}{2}\lambda b_2 b_3\right] \mp \frac{1}{\omega a b_5}\sqrt{\left(\frac{b_4}{2}\right)^2 - \left[\left(b_1\zeta_1 + \mu\zeta_3\Psi^2\Upsilon_1^2(\eta)\right)\omega a\right]^2} \tag{83}$$

3.3. Tuned spring-inerter-damper nonlinear vibration absorber (TSID-NVA)

The parameters of the NVA characterize the nonlinear frequency response function of the beam in Eq. (80), including the damping ratio ζ_3, mass ratio μ, and stiffness κ_1 and κ_3 in addition to the beam structural parameters and external excitation. Tuning these parameters could change the dynamics of the beam and the energy exchange between the beam and the NVA. One general application of the NVA is vibration reduction and control of the host structure it attaches to by absorbing, converting, and dissipating kinetic energy [8,24,39,40]. The energy absorption and dissipation capabilities of the proposed TSID-NVA substantially rely on these parameters of the NVA. Therefore, this subsection explores the nonlinear dynamics of the beam by tuning the parameters of the spring-inerter-damper NVA based on the nonlinear frequency response, specifically, the peak nonlinear frequency response of the beam. The backbone curve describing the peak nonlinear frequency response is extracted from the nonlinear frequency response function in Eq. (80) by taking the partial differentiation of the amplitude a with respect to the detuning parameter σ and setting $\frac{\partial a}{\partial \sigma} = 0$.

$$a = \sqrt{\frac{\sigma b_5 \omega}{\frac{3}{8}\left[\kappa_3\Upsilon_1^4(\eta)(1-\Psi)^4 - \frac{1}{2}\lambda b_2 b_3\right]}} \tag{84}$$

With the given system parameters, the backbone curve in Eq. (84) is the trajectory of the peak frequency responses over the varying excitation frequency (the detuning parameter σ). Combining Eq. (83) with (84) to eliminate the detuning parameter σ, one can obtain the peak nonlinear frequency response of the beam as

$$a_{peak} = \frac{b_4}{2\left[b_1\zeta_1 + \mu\zeta_3\Psi^2\Upsilon_1^2(\eta)\right]\omega} \tag{85}$$

Eq. (85) suggests that the resonant peak frequency response of the beam is a function of the excitation amplitude associated with b_4, damping ratio ζ_1 of the beam, damping ratio ζ_3 of the NVA, mass ratio μ, and the location parameter η of the NVA. By substituting Eq. (85) back into Eq. (84), one could get the detuning parameter corresponding to the bifurcation point or jumping down frequency. Interestingly, the peak nonlinear frequency response of the beam is independent of the nonlinear stiffness of the NVA. Another observation on Eq. (85) is that a_{peak} will degrade to the peak frequency response of the beam alone when either the mass ratio $\mu = 0$ or $\kappa_1 = 0$ ($\Psi = 0$), or both of them are zero, which is

$$a_{peak} = \frac{b_4}{2b_1\zeta_1\omega} \tag{86}$$

This is essentially the typical resonant frequency response function of a simplified single-degree-of-freedom (SDOF) beam, where b_1 and b_4 are dimensionless modal mass and modal force, respectively, as defined in Eq. (73). This indicates that the NVA has no contribution to the vibration absorption of the beam when either mass ratio $\mu = 0$ or $\kappa_1 = 0$, or both of them are zero, and the system regresses to the beam alone.

For vibration control, one of the widely used performance indexes is defined as the peak response of the system, i.e., a_{peak}. The minimization of this performance index is referred to as the H_∞ control [41]. Therefore, the parameters of the spring-inerter-damper NVA are usually desired to tune to the optimal values that minimize the peak frequency response of the beam to be controlled. Eq. (85) also shows that increasing the damping of both the beam and the NVA could effectively mitigate the resonant vibration of the beam. For the electromagnetic energy harvesting NVA, the damping is induced by the externally shunted electronics, usually simulated as a resistive load in the modeling [35]. Therefore, the damping of the NVA could be tuned by adjusting the external resistance in the circuit. However, it is necessary to clarify that the optimally tuned system for the best vibration reduction of the beam might not be optimal from the perspective of energy harvesting, aiming to maximize the power output. In turn, the optimally tuned NVA for the maximum power output might not be optimal for vibration reduction. A more detailed discussion from the perspectives of the optimal vibration reduction and energy harvesting respectively is referred to [42]. It is worth mentioning that the parameter Ψ is defined as a function of the linear stiffness κ_1 and the mass ratio μ of the NVA referred to the Subsection 3.1. Most importantly, it is observed that as $\omega = \sqrt{\frac{\kappa_1}{\mu}}$, $\Psi \to \infty$, which leads to $a_{peak} \to 0$. This implies the optimal parameters of the NVA should be tuned to satisfy $\omega = \sqrt{\frac{\kappa_1}{\mu}}$ for the effective vibration reduction of the beam. It is noted that $\sqrt{\frac{\kappa_1}{\mu}}$ is the dimensionless nominal frequency of the NVA. This means the nominal frequency of the NVA should be tuned to the natural frequency of the system to achieve the maximum reduction in the vibration amplitude. However, it should be emphasized here that the natural frequency ω of the system also depends on κ_1 and μ, according to the transcendental Eq. (60). Therefore, it's impossible to directly solve for the explicit expressions of the optimal NVA parameters by minimizing the resonant peak frequency response in Eq. (84) because of the involvement of the complex transcendental equation. Nevertheless, a parameter analysis could be numerically conducted to attain the optimal linear spring stiffness κ_1 and mass ratio μ of the spring-inerter-damper NVA given excitation amplitude and other system parameters.

4. Model verification, numerical results, and discussion

Numerical simulations were conducted in this section to verify the analytical nonlinear dynamics model and solutions of the beam-spring-inerter-damper system and to study the influence of system parameters on the dynamics. Otherwise stated, the dimensionless parameters used in the simulations are $\kappa_1 = \kappa_3 = 2\pi^4$, $\mu = 0.5$, $\zeta_1 = \zeta_2 = \zeta_3 = 0.05$, $\lambda = 1$, and $\eta = 0.3$. The direct numerical integration of the governing equations was conducted to validate the analytical solutions. The influence of the system parameters, particularly the parameters of the NVA, on the nonlinear frequencies, first mode shape, and nonlinear frequency responses of the BSID system are studied and discussed. The optimally tuned spring-inerter-damper NVA for the minimization of the peak frequency response is investigated and validated based on the numerical simulations.

4.1. Model verification

To verify the analytical solutions against the numerical simulation results, the governing equations of the system are decoupled and reduced to the first modal equation using the method of the separation of variables. The solutions are assumed to be $w_i = \sum_{n=1}^{\infty} Y_{in}(x) q_n(t)$, where $q_n(t)$ is the nth modal coordinate, n is the number of mode, $i = 1, 2$ are the number of the beam segments, and Y_{in} are the nth mode shapes in Eqs. (55) and (56). Substituting the solution into Eqs. (22) and (23), the governing equation of the beam can be reduced to the first modal vibration equation after some mathematical manipulation, which is given by

$$\ddot{q} + 2\zeta_1 \dot{q} + \omega^2 q - \lambda \frac{b_2 b_3}{2b_1} q^3 = \frac{b_4}{b_1} cos\Omega t \tag{87}$$

The subscript of the first modal coordinate is left out for simplicity. The cubic nonlinear term in the above equation is induced by the midplane stretching. Direct numerical integration was performed to the first modal equation at different excitation frequencies. The amplitudes of the time-domain steady-state responses are collected at every frequency point of interest and compared with the analytical nonlinear frequency responses. The nonlinear stiffness κ_3 and damping ζ_3 are ignored in the simulations since the reduced-order Eq. (87) doesn't consider the effect of the nonlinear boundary conditions at the NVA location. The zero initial conditions are used in the numerical simulations, as a consequence of which only one stable solution could be obtained in the multiple solution region. Fig. 2(a) presents the numerical simulation results and the analytical nonlinear frequency responses for $F_1 = F_2 = 0.3$ and three different values of the mass ratio μ, i.e. 0.001, 0.2, and 0.5. The numerical results perfectly agree with the analytical solutions when the mass ratio is very small (μ=0.001). However, the discrepancy emerges and becomes significant as the inertance increases. This is because Eq. (87) is obtained from the linear mode shapes, which don't consider the effect of the nonlinear boundary conditions at the NVA location. In contrast, the analytical model does include that as shown in Eqs. (68)-(70). As the inertance increases, the nonlinear boundary conditions become stronger and therefore are non-ignorable. As shown in Fig. 2 (a), ignoring the nonlinear boundary conditions could lead to serious underestimation of the nonlinear frequency responses in the numerical simulations.

To explain the discrepancy between the numerical and analytical results theoretically, the frequency response amplitude of the system is obtained from Eq. (87) by further neglecting the nonlinear term induced by the midplane stretching, which is given by

$$a = \sqrt{\frac{\left(\frac{b_4}{b_1}\right)^2}{(\omega^2 - \Omega^2)^2 + (2\zeta_1\omega)^2}} = \sqrt{\frac{\left(\frac{b_4}{2b_1}\right)^2}{(\sigma\omega)^2 + (\zeta_1\omega)^2}} \tag{88}$$

where the excitation frequency is assumed to be in the vicinity of the resonant frequency and can be written by $\Omega = \omega + \sigma$, which has been substituted into Eq. (88) and the small-term σ^2 is ignored. Similarly, neglecting the nonlinear stiffness and

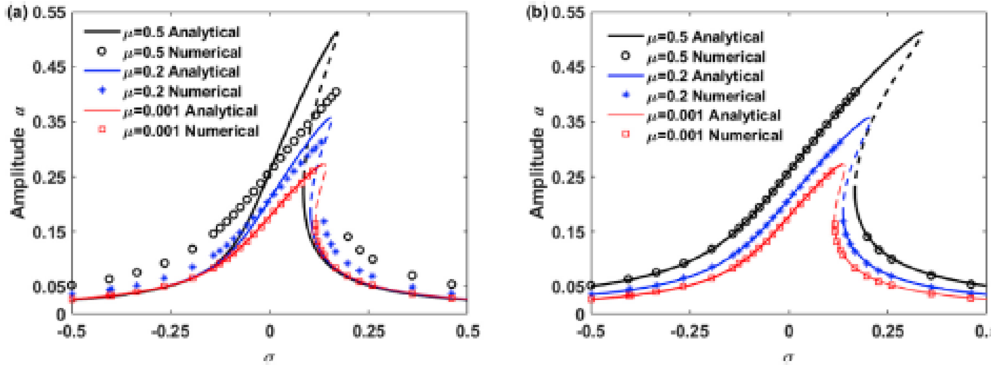

Fig. 2. Comparison of the numerical results and analytical solutions of the nonlinear frequency responses ($\kappa_1 = 2\pi^4, \kappa_3 = 0, \zeta_1 = \zeta_2 = 0.05, \zeta_3 = 0.0, \lambda = 1.0, \eta = 0.3$, and $F_1 = F_2 = 0.3$), (a) consider the nonlinear boundary condition effect in the analytical solutions, (b) ignore the nonlinear boundary condition effect in the analytical solutions.

Table 1
The linear natural frequencies ω (rad/s) of the BSID system with the spring-inerter-damper NVA at various locations (η) and the comparison with these of the BSM system.

η	1st mode		2nd mode		3rd mode		4th mode		5th mode	
	BSID	BSM[13]	BSID	BSM[13]	BSID	BSM[13]	BSID	BSM[13]	BSID	BSM[13]
0.0	9.87	9.87	39.48	39.48	88.83	88.83	157.91	157.91	246.74	246.74
0.1	9.29	10.98	(19.36)41.51	35.24	90.31	72.18	159.05	131.67	247.54	216.61
0.2	8.21	12.79	(20.36)44.69	32.25	91.01	76.08	158.36	150.55	246.74	246.74
0.3	7.37	14.30	(22.76)45.39	33.24	89.06	87.18	158.35	146.20	247.54	213.80
0.4	6.90	15.24	(25.95)42.17	36.75	89.65	82.04	159.07	136.33	246.74	246.74
0.5	6.75	15.55	(28.00)39.48	39.48	91.19	72.32	157.91	157.91	247.54	212.12

midplane stretching effect in the analytical nonlinear frequency response function in Eq. (80) and solving for the amplitude response, one has

$$a_{anl} = \sqrt{\frac{\left(\frac{b_4}{2b_1}\right)^2}{\left(\frac{b_5}{b_1}\sigma\omega\right)^2 + (\zeta\omega)^2}} = \sqrt{\frac{\left(\frac{b_4}{2b_1}\right)^2}{\left(\sigma\omega + \frac{\mu\kappa_1^2\Psi^2\Upsilon_1^2(\eta)}{b_1}\right)^2 + (\zeta_1\omega)^2}} \tag{89}$$

where $b_5 = b_1 + \mu\Psi^2\Upsilon_1^2(\eta)$ has been substituted into the above equation. Comparing Eq. (89) to Eq. (88), one can see one additional term $\frac{\mu\Psi^2\Upsilon_1^2(\eta)}{b_1}$ is included in the analytical solution in Eq. (89). This term is actually from the coefficient b_5 and is originated from the nonlinear boundary conditions in Eq. (70). By setting the second term in the coefficient b_5 to zero, the effect of the nonlinear boundary conditions in the analytical solutions is ignored, and the deteriorated analytical solutions are plotted in Fig. 2(b) together with the numerical results. It is noted that the neglect of the midplane stretching effect in Eqs. (88) and (89) is to derive the explicit expression of the frequency response for an intuitive comparison. The numerical and analytical results in Fig. 2(b) include the midplane stretching effect. As expected, the numerical results almost perfectly match the analytical solutions without considering the nonlinear boundary conditions. This implies that the presented analytical nonlinear dynamics model and solutions are more accurate because of the involvement of the nonlinear boundary conditions at the NVA location, particularly for a large inertance.

4.2. Natural frequencies and mode shapes

This subsection studies the influence of the system parameters on the system's natural frequencies and mode shapes. The natural frequency $\omega = \beta^2$ of the BSID system is firstly derived by numerically solving the transcendental Eq. (60). The first five natural frequencies of the BSID system with the NVA deployed at different locations (varying η) are presented in Table 1, and compared with these of the typical beam-spring-mass (BSM) system in literature [13]. As the geometrical symmetry of the system, the results are only presented for the cases of $\eta \leq 0.5$. At $\eta = 0$, the NVA is located at the left support position and thus does not affect the beam dynamics, which means both the BSID and BSM systems degenerate to the simply-supported beam alone. In such a case, the first five natural frequencies of the BSID system are the same as these of the BSM system in Ref.[13], as presented in the first row of Table 1. This agreement further validates the correctness and

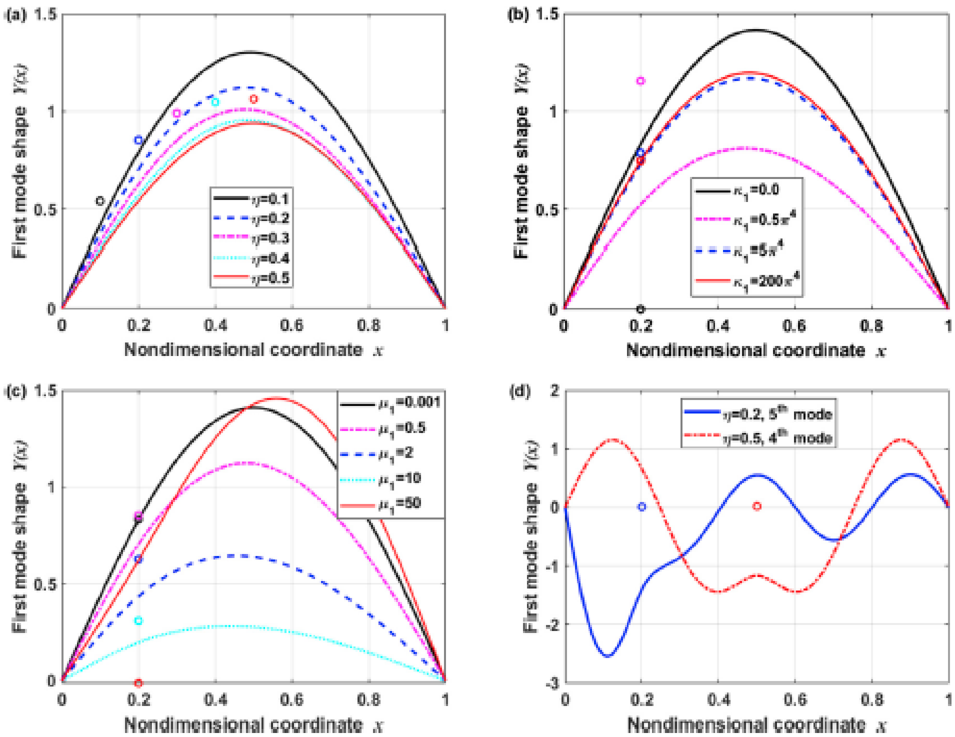

Fig. 3. The influence of (a) the spring-inerter-damper location on the first mode shape($\kappa_1 = 2\pi^4$ and $\mu = 0.5$), (b)the linear spring stiffness ($\eta = 0.2$ and $\mu = 0.5$), and (c) the inertia mass ($\kappa_1 = 2\pi^4$ and $\eta = 0.2$),(d) the 5th mode shape for $\eta = 0.2$ and the 4th mode shape for $\eta = 0.5$ ($\kappa_1 = 2\pi^4$ and $\mu = 0.5$).

accuracy of the presented model. In contrast with the increasing trend in the first natural frequency of the BSM system, the first natural frequency of the BSID system decreases as the NVA shifts to the middle point of the beam. Furthermore, another mode of the NVA vibration emerges between the first and the second beam vibration modes, the natural frequencies of which are given in the parentheses along with the second beam vibration frequencies. The BSID system has higher natural frequencies than the BSM system for the higher modes apart from these highlighted in gray. Interestingly, it is found that the second and fourth natural frequencies of the two systems for $\eta = 0.5$, the fifth natural frequencies for $\eta = 0.2$ and 0.4, are identical with the these of the simply-supported beam alone. This implies that neither the proposed spring-inerter-damper NVA nor the typical spring-mass NVA influences the second and fourth natural frequencies when $\eta = 0.5$, and the fifth natural frequency when $\eta = 0.2$ and 0.4. This is because these locations are either the strain nodes of the mode shapes or the NVA mode. These findings provide a basis for the design of the BSID system, especially for the specific modal control of the beam vibration.

The first mode shape of the proposed BSID system is derived from Eqs. (55) and (56) and plotted in Fig. 3 (a) for the varying NVA location (η), Fig. 3(b) for the varying linear stiffness (κ_1), and Fig. 3 (c) for the varying inertia mass (μ). The circular markers indicate the mode shape of the NVA. Fig. 3 (a) shows that the location of the NVA has a remarkable influence on the first mode shape of the beam. The first mode shape is not symmetric about the middle point of the beam any longer like that of a general simply-supported beam except for $\eta = 0.5$ (NVA at the midpoint of the beam). Instead, it shifts to the right hand as the location parameter η increases from 0.1 to 0.4 (the NVA moves to the right side). The influence of the NVA on the first mode shape of the left half segment is more significant than on that of the right half segment because the NVA is deployed within the left half segment of the beam. These findings conclude that the spring-inerter-damper NVA has a slight impact on the first mode shape of the simply-supported beam when deployed at the midpoint ($\eta = 0.5$) but can significantly differ first mode shape when installed at the locations away from the midpoint.

The linear stiffness κ_1 of the spring exhibits remarkable influence on the vibration mode of the NVA but the slight impact on the first mode shape of the beam, as shown in Fig. 3(b). There will be no linear vibration for NVA when $\kappa_1 = 0.0$ and the NVA has no influence on the first mode shape of the beam. The NVA shows a large amplitude vibration when a soft spring is used, i.e., $\kappa_1 = 0.5\pi^4$, and the first mode shape of the beam is slightly shifted to the left-hand side. When the linear stiffness of the NVA becomes much larger ($\kappa_1 = 5.0\pi^4$) compared with the beam stiffness, the connection between

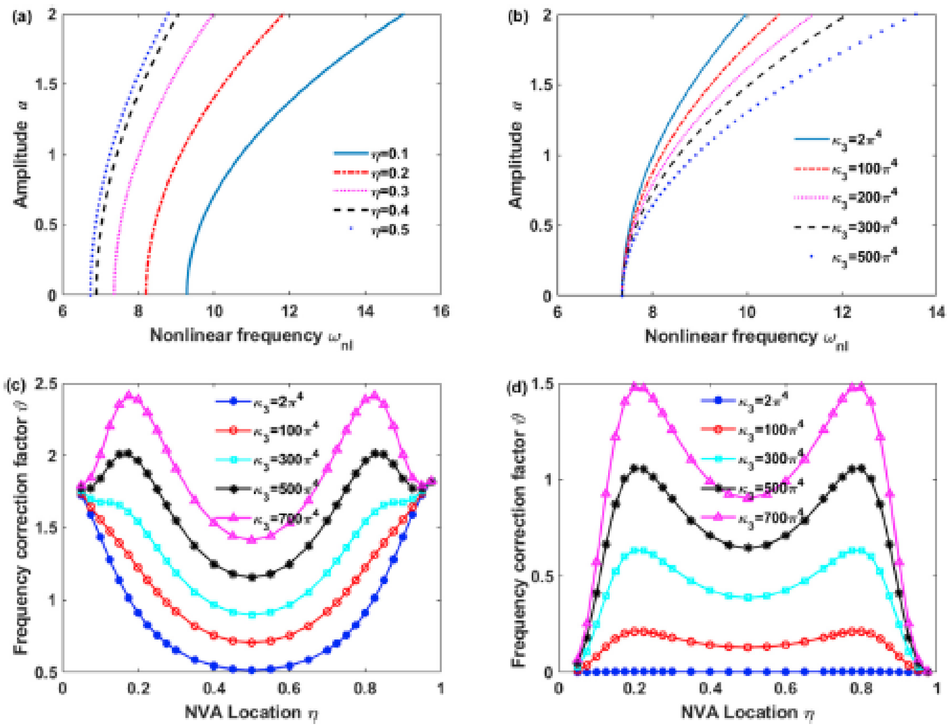

Fig. 4. Variation of the nonlinear frequency with vibration amplitude a (a) various η : $\kappa_1 = \kappa_3 = 2\pi^4, \mu = 0.5, \zeta_1 = \zeta_2 = \zeta_3 = 0, F_1 = F_2 = 0$; (b) various nonlinear stiffness κ_3 : $\kappa_1 = 2\pi^4, \mu = 0.5, \eta = 0.3, \zeta_1 = \zeta_2 = \zeta_3 = 0, F_1 = F_2 = 0$; (c) frequency correction factor ϑ with the midplane stretching: $\kappa_1 = 2\pi^4, \mu = 0.5, \zeta_1 = \zeta_2 = \zeta_3 = 0, F_1 = F_2 = 0$; (d) frequency correction factor ϑ without the midplane stretching: $\kappa_1 = 2\pi^4, \mu = 0.5, \zeta_1 = \zeta_2 = \zeta_3 = 0, F_1 = F_2 = 0$.

the NVA and the beam close to rigidity, and thus the NVA always vibrates along with the beam. The vibration mode of the NVA is completely the same with the beam at the installation position as the linear stiffness further increases, e.g., $\kappa_1 = 200\pi^4$. Fig. 3 (c) suggests that the inertial mass also has a remarkable effect on the first mode of the beam and the NVA. When the inertial mass is minimal ($\mu = 0.001$), the NVA follows the beam vibration at the installation location and fails to reduce the beam vibration. The first mode shape of the beam slightly skews to the left-hand side as the inertial mass increases. The beam vibration cannot bring the NVA in motion any more as the inertial mass becomes huge, e.g., $\mu = 50$, and the beam vibration mode is notably changed by the stronger constraint of the NVA due to the large inertial mass. As an example, Fig. 3 (d) plots the fifth mode shape for $\eta = 0.2$ and the fourth mode shape for $\eta = 0.5$ to demonstrate that the NVA vibration modes are nodes and, therefore, the corresponding frequencies of the system are the same with the these of the beam alone, as shown with the gray background in Table 1. These results demonstrate that the mode shapes of the beam could be changed to varying degrees by the NVA with different parameters and locations. This influence of the NVA parameters and location on the mode shapes of the beam was not considered in most studies that modeled the beam as a continuous one using the mode shapes of a typical simply-supported beam, but can result in significant errors.

4.3. Nonlinear frequencies

The nonlinear frequencies ω_{nl} are calculated with respect to the vibration amplitude from Eq. (79) for various values of the NVA location parameter η and the nonlinear stiffness κ_3, which are plotted in Fig. 4(a) and (b), respectively. The results show that the position of the NVA has a prominent influence on the nonlinear frequency of the BSID system. The nonlinear frequency and the nonlinearity of the system decrease as the NVA shifts to the center of the beam. This result is contrary to the findings of the typical BSM system [13], where the system has the maximum nonlinear frequency and highest nonlinearity when the NVA locates at the midpoint of the beam. The nonlinear stiffness κ_3 of the NVA also significantly contributes to the variation of the nonlinear frequency. Fig. 4(b) suggests that the nonlinear frequency increases along with the nonlinear stiffness at the same vibration amplitude. The increment of the nonlinear frequency induced by the nonlinear stiffness κ_3 is even more significant as the frequency response amplitude a becomes larger. Fig. 4 (c) plots the nonlinear frequency correction factor ϑ, which gives more intuitive evidence on the contributions of the location parameter η and the nonlinear

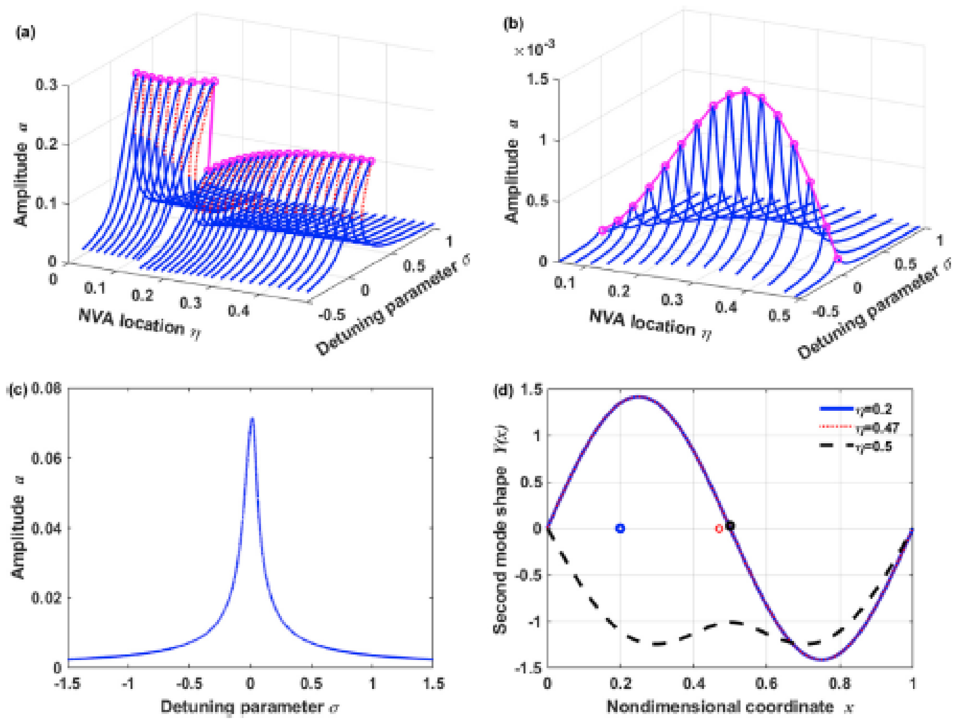

Fig. 5. Frequency response curves with different values of the location parameter η (a) first mode; (b) second mode for $\eta = 0 \sim 0.49$; (c) second mode for $\eta = 0.5$; (d) second mode shapes of the system; ($\kappa_1 = 0.2\pi^4, \kappa_3 = 2\pi^4, \mu = 0.5, \zeta_1 = \zeta_2 = \zeta_3 = 0.05, F_1 = F_2 = 0.3$).

stiffness κ_3 of the NVA to the nonlinear frequency. The nonlinear frequency correction factor is almost the same when NVA is near to the ends of the beam for different values of the nonlinear stiffness κ_3, which implies the nonlinear stiffness of the NVA has little effect and weak contributions to the system nonlinearity, which is dominated by the midplane stretching effect. As the NVA moves to the middle of the beam, the nonlinear frequency correction factor shows a decreasing trend for a small nonlinear stiffness κ_3. However, as the nonlinear stiffness increases ($\kappa_3 > 300\pi^4$), the frequency correction factor has an increasing trend in $0 < \eta < 0.2(0.8 < \eta < 1.0)$ and decreasing trend in $0.2 < \eta < 0.5(0.5 < \eta < 0.8)$. This change in the trend of the frequency correction factor is because the nonlinear stiffness κ_3 gradually dominates the nonlinearity of the system as it increases.

To study the influence of the midplane stretching on the nonlinearity, Fig. 4 (d) plots the frequency correction factor for different values of κ_3 without the consideration of the midplane stretching effect. Comparing Fig. 4 (d) with (c), one can find that the frequency correction factor curve over different NVA locations along the length of the beam is smaller and maintains the M shape in Fig. 4 (d). But the curve in Fig. 4 (c) has a U shape for a smaller κ_3 and gradually turns to the M shape as κ_3 increases. This reveals that the nonlinearity is dominated by the midplane stretching effect when κ_3 is smaller. But when it increases (i.e.> $300\pi^4$), the nonlinear stiffness κ_3 gradually becomes dominant. Eq. (78) can also explain this, which shows the frequency correction factor is composed of two terms that are respectively associated with the nonlinear stiffness κ_3 and the midplane stretching induced coefficient b_2.

4.4. Nonlinear frequency response

The nonlinear frequency response curves are derived by numerically solving Eq. (80) with the given detuning parameter σ and the excitation amplitudes of $F_1 = F_2 = 0.3$. The dimensionless damping ratios of $\zeta_1 = \zeta_2 = 0.05$ for the beam structure and $\zeta_3 = 0.05$ for the NVA are used in the simulations. A smaller linear stiffness of $\kappa_1 = 0.2\pi^4$ is chosen to tune the nominal frequency $\sqrt{\frac{\kappa_1}{\mu}}$ of the NVA close to the first natural frequency of the BSID system for better vibration reduction performance. Fig. 5(a) and (b) shows the first and second mode nonlinear frequency response curves for the cases that the spring-inerter-damper NVA is installed at various locations. The solid lines are stable solutions, while the dashed lines are unstable solutions determined by the eigenvalues of the Jacobian matrix in Eq. (82). The curves with circular markers are the trajectories of the peak nonlinear frequency responses. A minimum is observed at the location near $\eta = 0.15$, which

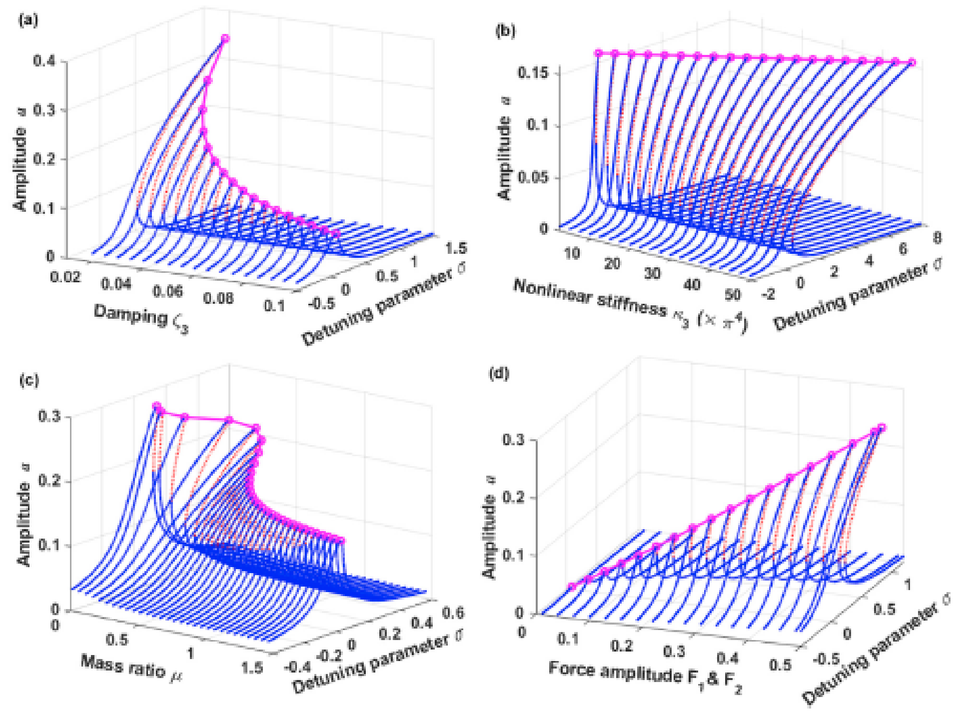

Fig. 6. Influence of the damping coefficient $\zeta_3(\kappa_3 = 2\pi^4, \mu = 0.5)$, nonlinear stiffness $\kappa_3(\zeta_3 = 0.05, \mu = 0.5)$, and inertial mass ratio $\mu(\kappa_3 = 2\pi^4, \zeta_3 = 0.05)$ on the first mode frequency response curves: $\kappa_1 = 0.2\pi^4$, $\zeta_1 = \zeta_2 = 0.05$, $\eta = 0.3$, $F_1 = F_2 = 0.3$.

suggests that the beam vibration is mostly reduced by the NVA deployed at this location and is thus termed as the optimal position. Scrutiny at this location reveals that the first natural frequency of the system is 5.82, which is close to the nominal natural frequency of the NVA, i.e., $\sqrt{\frac{\kappa_1}{\mu}} = 6.24$. According to the analysis in Subsection 3.3, the beam vibration could be well reduced as the nominal natural frequency of the NVA is close to the natural frequency of the system.

For the second mode vibrations, only the frequency responses of the system with $\eta = 0.0 \sim 0.49$ are plotted in Fig. 5(b) since the frequency responses for η close to 0.5 is much larger and is therefore separately plotted in Fig. 5(c) for a better view. The second mode frequency response curves show almost no nonlinearity. The peak value of the second mode frequency response increases firstly and then reaches an extremum at $\eta = 0.35$ and then gradually decreases. All the second mode frequency responses are much smaller compared with the first mode responses in Fig. 5(a), which implies that the second mode vibration is ignorable when the system subjects to the excitation in the vicinity of the primary frequency. The amplitude of the second mode vibration at $\eta = 0.5$ as plotted in Fig. 5(c) is much larger than these in Fig. 5(b) for $\eta = 0.0 \sim 0.49$ but still much smaller than that of the first mode vibration. This is because the second mode shape of the beam is significantly changed when $\eta = 0.5$ and is quite different from these when $\eta = 0.0 \sim 0.49$. As an example, Fig. 5(d) plots the second mode shapes of the system for η=0.2, 0.47, and 0.5, which shows the difference.

The influence of the other system parameters, including the damping ratios, nonlinear stiffness κ_3, and the mass ratio μ on the frequency responses, are also explored in this subsection. The nonlinear frequency responses of the BSID system with different damping of the NVA are plotted in Fig. 6(a). The vibration of the beam decreases as the damping ratio ζ_3 becomes larger because the damper dissipates more energy in the NVA as the damping ratio increases. The quick drop in the peak nonlinear frequency response along with the augment of damping ζ_3, as shown by the thick curve with the circular markers, is consistent with the analytical analysis in Subsection 3.3 based on Eq. (85). The nonlinear frequency curve shows stronger nonlinearity by increasingly bending to the right-hand side as the nonlinear stiffness κ_3 becomes larger, as shown in Fig. 6(b). As expected and found in Subsection 3.3, the resonant peak nonlinear frequency response keeps unchanged with the varying nonlinear stiffness κ_3 of the NVA. The mass ratio μ has a great effect on the nonlinear dynamics of the beam, as shown in Fig. 6(c), which suggests that the nonlinear frequency response of the system decreases as the mass ratio μ increases. It is found that the nominal frequency $\sqrt{\frac{\kappa_1}{\mu}}$ of the NVA is much larger than the first natural frequency ω of the system when the mass ratio is smaller and thus the vibration reduction performance is worse. As the mass ratio increases,

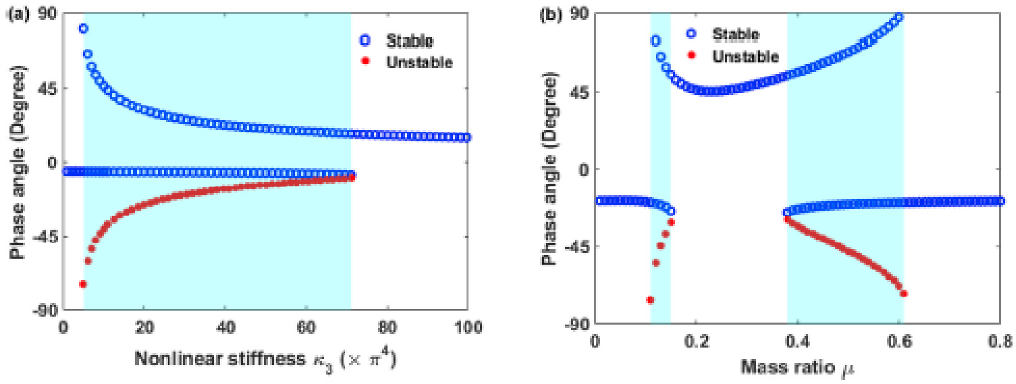

Fig. 7. Bifurcation diagram and the phase angle with respect to the (a) nonlinear stiffness κ_3 ($\eta = 0.3, \kappa_1 = 0.2\pi^4, \kappa_3 = 2\pi^4, \mu = 0.5, \zeta_1 = \zeta_2 = \zeta_3 = 0.05, F_1 = F_2 = 0.5, \sigma = 0.5$); (b) mass ratio μ ($\eta = 0.3, \kappa_1 = 0.2\pi^4, \kappa_3 = 2\pi^4, \zeta_1 = \zeta_2 = \zeta_3 = 0.05, F_1 = F_2 = 0.5, \sigma = 0.16$).

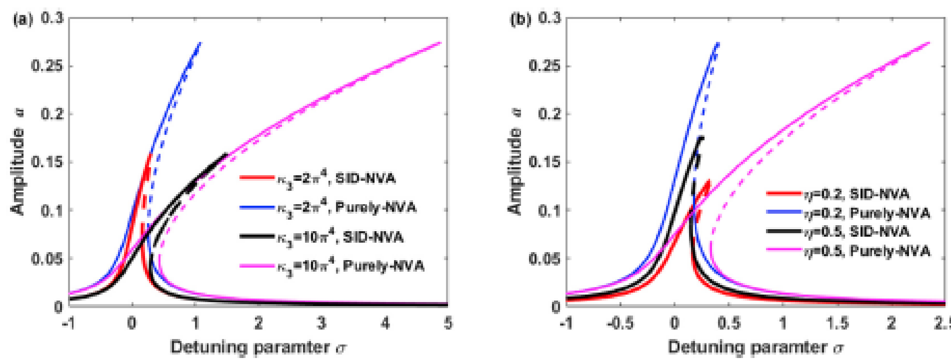

Fig. 8. Performance comparison with the purely NVA ($\kappa_1 = 0.2\pi^4, \mu = 0.5, \zeta_1 = \zeta_2 = \zeta_3 = 0.05, F_1 = F_2 = 0.3$). (a) $\eta = 0.3$; (b) $\kappa_3 = 2\pi^4$.

both the nominal frequency of the NVA and the first natural frequency of the system reduce and get closer with each other, and therefore the vibration is significantly reduced. Fig. 6(d) suggests that both the frequency response and nonlinearity of the beam increase as the excitation amplitude aggrandizes. The resonant peak nonlinear frequency responses indicated by the line with circular markers rises linearly along with the increasing excitation amplitude, which follows the observation from Eq. (85) because the contribution of the excitation amplitude is reflected in the numerator b_4 of the peak frequency response function a_{peak}.

The effect of the parameters of the NVA on the system dynamics can also be studied by the bifurcation diagrams [19] and the phase angle derived in Eq. (85) in additional to the nonlinear frequency response. As an example, the phase angle of the system at the varying nonlinear stiffness κ_3 is plotted in Fig. 7(a) for the given detuning parameter σ=0.5 at the excitation amplitude of $F_1 = F_2 = 0.5$. It shows that only one stable solution exists when the nonlinear stiffness κ_3 is very small because the system nonlinearity is very weak, and thus there is only one lower-branch solution at the given detuning frequency, as shown in Fig. 6(b). As the nonlinear stiffness increases, the system nonlinearity gradually becomes stronger, which is reflected in the more severe bend of the frequency response curve, as shown in Fig. 6(b). As the frequency bends more to the right-hand side, three solutions, including two stable ones at the higher and lower branches and one unstable one, emerge at the given detuning frequency. The dark background in Fig. 7(a) shows the nonlinear stiffness range that the system has multiple solutions. The bifurcation diagram over the varying mass ratio is plotted in Fig. 7(b) for the detuning parameter σ=0.16 at the same excitation amplitude of $F_1 = F_2 = 0.5$. The results show that the mass ratio has a more complex influence on the nonlinear dynamics of the system. The system has multiple solutions at the selected detuning frequency in two different ranges of the mass ratio as marked in dark backgrounds in Fig. 7(b).

The vibration reduction performance of the proposed spring-inerter-damper NVA (SID-NVA) is evaluated by comparing with that of the purely nonlinear vibration absorber (Purely-NVA), which only has the nonlinear stiffness component, and therefore the linear stiffness κ_1 is set to zero. The nonlinear frequency responses of the system with the proposed SID-NVA and the Purely-NVA are plotted in Fig. 8(a) for $\kappa_3 = 2\pi^4$ and $10\pi^4$, respectively. The proposed SID-NVA exhibits much better vibration reduction capability than the Purely-NVA for the considered two different values of the nonlinear stiffness,

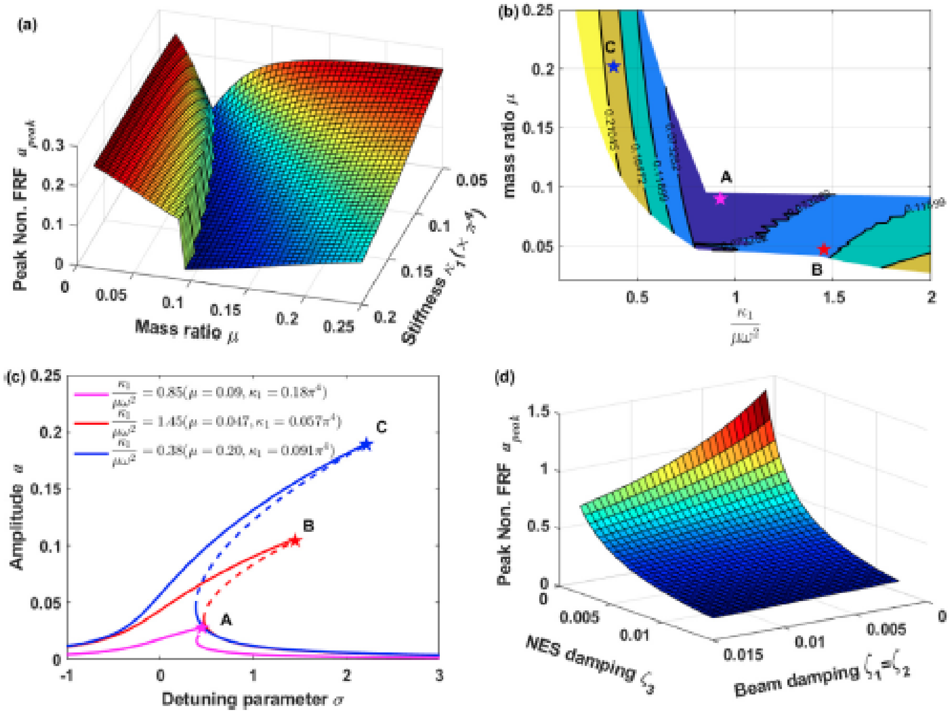

Fig. 9. Peak nonlinear frequency responses vs. (a) varying linear stiffness κ_1 and mass ratio μ; (b) contour plot with varying $\frac{\kappa_1}{\mu\omega^2}$ and μ; (c) frequency response for the cases of $\frac{\kappa_1}{\mu\omega^2} \approx 1$, $\frac{\kappa_1}{\mu\omega^2} > 1$, and $\frac{\kappa_1}{\mu\omega^2} < 1$; ($\kappa_3 = 2\pi^4, \zeta_1 = \zeta_2 = 0.02, \zeta_3 = 0.005, \eta = 0.3, F_1 = F_2 = 1$); (d) varying damping of the beam ($\zeta_1 = \zeta_2$) and the NVA (ζ_3).

The comparison is also carried out for different NVA locations. Fig. 8(b) plots the nonlinear frequency responses of the two systems for $\eta = 0.2$ and 0.5, respectively. The SID-NVA outperforms the Purely-NVA in the vibration suppression at both locations.

4.5. Peak nonlinear frequency response with the tuned spring-inerter-damper NVA

To find the optimal tuning parameters of the NVA, the peak nonlinear frequency responses of the beam are computed from Eq. (85) and presented in Fig. 9(a) for the varying mass ratio μ and linear stiffness κ_1. All the other system parameters and the excitations remain unchanged as previously declared. It can be seen that there is always an optimal combination of the two parameters μ and κ_1 in the range of interest that is corresponding to the minimum of the peak nonlinear frequency responses. Fig. 9(b) gives the contour plot of the peak nonlinear frequency response for different mass ratio and $\frac{\kappa_1}{\mu\omega^2}$ for a clearer view on the optimal tuning parameters as well as the associated minimum resonant peak. The smallest peak nonlinear frequency response is observed at the region that $\frac{\kappa_1}{\mu\omega^2}$ is close to 1, i.e. $\omega \approx \sqrt{\frac{\kappa_1}{\mu}}$. This numerical simulation result complies with the conclusion drawn in the Subsection 3.3 that the optimal parameters of the mass ratio μ and linear stiffness κ_1 of the NVA need to satisfy $\omega = \sqrt{\frac{\kappa_1}{\mu}}$ for the maximum reduction in beam vibration. It is worth noting that there is a jump in the peak response of the beam as the mass ratio increases in the range of $0.05 \sim 1.0$, which is corresponding to the indentions in the contour plot in Fig. 9(b). This is because as the mass ratio increases in such a range $\sqrt{\frac{\kappa_1}{\mu}}$ gradually approaches to ω, but it cannot be exactly tuned to equal to ω which would place the transcendental Eq. (60) in an ill condition (the denominator $(\kappa_1 - \mu\beta^4)$ approaches to zero). To further intuitively demonstrate this conclusion, the nonlinear frequency responses of the beam with three different combinations of the two parameters μ and κ_1, corresponding to the parameter regions marked by the pentagrams at A, B, and C points in Fig. 9(b), are plotted in Fig. 9(c). The three combinations of the two parameters are deliberately chosen to represent three typical cases of the NVA that are corresponding to $\frac{\kappa_1}{\mu\omega^2} \approx 1$, $\frac{\kappa_1}{\mu\omega^2} > 1$, and $\frac{\kappa_1}{\mu\omega^2} < 1$. The corresponding peak nonlinear frequency responses are also marked by the pentagrams along with the capital letters A, B, and C in Fig. 9(c). The results suggest that case A with the parameters of the NVA satisfying $\frac{\kappa_1}{\mu\omega^2} \approx 1$ has the smallest frequency response compared with the other two cases. This further confirms the analytical analysis that the parameters should be optimally tuned to make the nominal frequency of the NVA close to the system's natural frequency to achieve the best vibration control of the beam. It is worth mentioning that the natural frequency ω is also dependent on the two tuning parameters studied here.

Fig. 9 (d) presents the peak nonlinear frequency response of the beam with respect to different damping ratios $\zeta_1 = \zeta_2$ of the beam structure and ζ_3 of the NVA. It shows that the peak nonlinear frequency response drops rapidly as either or both of the damping ratios of the beam and NVA increase, which is also in accordance with the analysis in the Subsection 3.3 and the results in Fig. 6(a). This is because significant damping enhances the energy dissipation capability of the NVA. Therefore, it concludes that increasing the damping of the spring-inerter-damper NVA could be an effective way to reduce the vibration of the beam in addition to enlarge the damping of the beam structure.

5. Conclusion

This paper studies the exact nonlinear dynamics of a simply-supported beam with a nonlinear spring-inerter-damper vibration absorber (NVA). A two-terminal electromagnetic rotational inerter device is used to replace the mass and damping elements in the typical NVA to reduce the physical mass. Unlike most existing studies employing the mode shapes of the simply-supported beam alone, this study considers the abrupt changes in the boundary conditions at the NVA location and the midplane stretching of the primary beam to develop an exact nonlinear dynamics model for the beam-spring-inerter-damper system. The system governing equations are derived from the energy method and directly solved by the method of multiple scales for the approximate analytical solutions. The analytical model was verified with the simulation results obtained by numerically integrating the governing equations. The results demonstrate that neglecting the nonlinear boundary conditions at the spring-inerter-damper location results in severe underestimation of the nonlinear frequency responses. The influence of the parameters and location of the NVA on the nonlinear dynamics of the beam, including natural frequencies, nonlinear frequency correction factor, nonlinear frequency responses, and vibration reduction performance, is studied and discussed. The optimal tuning condition of the NVA is analytically found to minimize the peak nonlinear frequency response of the primary beam.

The location of the NVA has an evident influence on the natural frequencies of the system except for these near to the strain nodes of the mode shapes. The NVA has a slight impact on the first mode shape of the beam when installed at the midpoint but can significantly differ when installed at the locations away from the midpoint. The nonlinear stiffness of the NVA enhances the system nonlinearity but has no contribution to the peak nonlinear frequency response of the beam. The optimally tuned NVA could significantly reduce the peak nonlinear frequency response of the beam, and the optimal tuning condition is analytically formulated and numerically verified. A comparison study on the peak nonlinear frequency responses of the beam with various parameters of the NVA further validated the analytical analysis.

Declaration of Competing Interest

The authors certify that they have NO affiliations with or involvement in any organization or entity with any financial interest (such as honoraria; educational grants; participation in speakers' bureaus; membership, employment, consultancies, stock ownership, or other equity interest; and expert testimony or patent-licensing arrangements), or non-financial interest (such as personal or professional relationships, affiliations, knowledge or beliefs) in the subject matter or materials discussed in this manuscript.

CRediT authorship contribution statement

Feng Qian: Conceptualization, Methodology, Formal analysis, Investigation, Data curation, Writing - original draft, Writing - review & editing. **Lei Zuo:** Supervision, Writing - review & editing, Project administration.

Acknowledgement

The authors gratefully acknowledge the financial support from the National Science Foundation (Award Numbers: 1935951).

References

[1] D. Kremer, K. Liu, A nonlinear energy sink with an energy harvester: transient responses, J. Sound Vib. 333 (20) (2014) 4859–4880.
[2] D. Kremer, K. Liu, A nonlinear energy sink with an energy harvester: harmonically forced responses, J. Sound Vib. 410 (2017) 287–302.
[3] A.F. Vakakis, O.V. Gendelman, L.A. Bergman, D.M. McFarland, G. Kerschen, Y.S. Lee, Nonlinear targeted energy transfer in mechanical and structural systems, volume 156, Springer Science & Business Media, 2008.
[4] H. Ding, L.-Q. Chen, Designs, analysis, and applications of nonlinear energy sinks, Nonlinear Dyn. 100 (2020) 3061–3107.
[5] M. Parseh, M. Dardel, M.H. Ghasemi, Investigating the robustness of nonlinear energy sink in steady state dynamics of linear beams with different boundary conditions, Commun. Nonlinear Sci. Numer. Simul. 29 (1–3) (2015) 50–71.
[6] X. Jiang, D.M. McFarland, L.A. Bergman, A.F. Vakakis, Steady state passive nonlinear energy pumping in coupled oscillators: theoretical and experimental results, Nonlinear Dyn. 33 (1) (2003) 87–102.

[7] X.-Y. Mao, H. Ding, L.-Q. Chen, Nonlinear torsional vibration absorber for flexible structures, J. Appl. Mech. 86 (2) (2019).
[8] Y.-W. Zhang, S. Hou, K.-F. Xu, T.-Z. Yang, L.-Q. Chen, Forced vibration control of an axially moving beam with an attached nonlinear energy sink, Acta Mech. Solida Sin. 30 (6) (2017) 674–682.
[9] Y. Starosvetsky, O. Gendelman, Interaction of nonlinear energy sink with a two degrees of freedom linear system: internal resonance, J. Sound Vib. 329 (10) (2010) 1836–1852.
[10] G. Sigalov, O. Gendelman, M. Al-Shudeifat, L. Manevitch, A.F. Vakakis, L. Bergman, Resonance captures and targeted energy transfers in an inertially-coupled rotational nonlinear energy sink, Nonlinear Dyn. 69 (4) (2012) 1693–1704.
[11] Y.-Y. Chen, Z.-C. Qian, W. Zhao, C.-M. Chang, A magnetic bi-stable nonlinear energy sink for structural seismic control, J. Sound Vib. 473 (2020) 115233.
[12] J. Taghipour, M. Dardel, Steady state dynamics and robustness of a harmonically excited essentially nonlinear oscillator coupled with a two-dof nonlinear energy sink, Mech. Syst. Sig. Process. 62 (2015) 164–182.
[13] M. Pakdemirli, A. Nayfeh, Nonlinear vibrations of a beam-spring-mass system, J. Vib. Acoust. 116 (1994) 433–439.
[14] E. Özkaya, M. Pakdemirli, H. Öz, Non-linear vibrations of a beam-mass system under different boundary conditions, J. Sound Vib. 199 (4) (1997) 679–696.
[15] F. Georgiades, A.F. Vakakis, Dynamics of a linear beam with an attached local nonlinear energy sink, Commun. Nonlinear Sci. Numer. Simul. 12 (5) (2007) 643–651.
[16] F.S. Samani, F. Pellicano, A. Masoumi, Performances of dynamic vibration absorbers for beams subjected to moving loads, Nonlinear Dyn. 73 (1–2) (2013) 1065–1079.
[17] M.O. Chtiba, S. Choura, A. Nayfeh, S. El-Borgi, Vibration confinement and energy harvesting in flexible structures using collocated absorbers and piezoelectric devices, J. Sound Vib. 329 (3) (2010) 261–276.
[18] M. Parseh, M. Dardel, M.H. Ghasemi, Performance comparison of nonlinear energy sink and linear tuned mass damper in steady-state dynamics of a linear beam, Nonlinear Dyn. 81 (4) (2015) 1981–2002.
[19] M. Parseh, M. Dardel, M.H. Ghasemi, M.H. Pashaei, Steady state dynamics of a non-linear beam coupled to a non-linear energy sink, Int. J. Non Linear Mech. 79 (2016) 48–65.
[20] G. Failla, On the dynamics of viscoelastic discontinuous beams, Mech Res Commun 60 (2014) 52–63.
[21] M. Bukhari, O. Barry, Exact nonlinear dynamic analysis of a beam with a nonlinear vibration absorber and with various boundary conditions, J. Comput. Nonlinear Dyn. 15 (1) (2020).
[22] Y. Starosvetsky, O. Gendelman, Vibration absorption in systems with a nonlinear energy sink: nonlinear damping, J. Sound Vib. 324 (3–5) (2009) 916–939.
[23] J. Chen, W. He, W. Zhang, M. Yao, J. Liu, M. Sun, Vibration suppression and higher branch responses of beam with parallel nonlinear energy sinks, Nonlinear Dyn. 91 (2) (2018) 885–904.
[24] M. Kani, S. Khadem, M. Pashaei, M. Dardel, Vibration control of a nonlinear beam with a nonlinear energy sink, Nonlinear Dyn. 83 (1–2) (2016) 1–22.
[25] J. Chen, W. Zhang, M. Yao, J. Liu, Vibration suppression for truss core sandwich beam based on principle of nonlinear targeted energy transfer, Compos. Struct. 171 (2017) 419–428.
[26] J. Zang, T.-C. Yuan, Z.-Q. Lu, Y.-W. Zhang, H. Ding, L.-Q. Chen, A lever-type nonlinear energy sink, J. Sound Vib. 437 (2018) 119–134.
[27] J. Zang, R.-Q. Cao, B. Fang, Y.-W. Zhang, A vibratory energy harvesting absorber using integration of a lever-enhanced nonlinear energy sink and a levitation magnetoelectric energy harvester, J. Sound Vib. (2020) 115534.
[28] F. Qian, Y. Luo, H. Sun, W.C. Tai, L. Zuo, Optimal tuned inerter dampers for performance enhancement of vibration isolation, Eng. Struct. 198 (2019) 109464.
[29] K. Ikago, K. Saito, N. Inoue, Seismic control of single-degree-of-freedom structure using tuned viscous mass damper, Earthq. Eng. Struct. Dyn. 41 (3) (2012) 453–474.
[30] X. Feng, X. Jing, Z. Xu, Y. Guo, Bio-inspired anti-vibration with nonlinear inertia coupling, Mech. Syst. Sig. Process. 124 (2019) 562–595.
[31] A. Javidialesaadi, N.E. Wierschem, An inerter-enhanced nonlinear energy sink, MMech. Syst. Sig. Process. 129 (2019) 449–454.
[32] Y.-W. Zhang, Y.-N. Lu, W. Zhang, Y.-Y. Teng, H.-X. Yang, T.-Z. Yang, L.-Q. Chen, Nonlinear energy sink with inerter, Mech. Syst. Sig. Process. 125 (2019) 52–64.
[33] H.-Y. Chen, X.-Y. Mao, H. Ding, L.-Q. Chen, Elimination of multimode resonances of composite plate by inertial nonlinear energy sinks, Mech. Syst. Sig. Process. 135 (2020) 106383.
[34] X. Jin, M.Z. Chen, Z. Huang, Suppressing random response of a regular structure by an inerter-based dynamic vibration absorber, J. Vib. Acoust. 141 (4) (2019).
[35] Y. Pan, T. Lin, F. Qian, C. Liu, J. Yu, J. Zuo, L. Zuo, Modeling and field-test of a compact electromagnetic energy harvester for railroad transportation, Appl. Energy 247 (2019) 309–321.
[36] Z.N. Ahmadabadi, S. Khadem, Nonlinear vibration control of a cantilever beam by a nonlinear energy sink, Mech. Mach. Theory 50 (2012) 134–149.
[37] Z. Zhang, Z.-Q. Lu, H. Ding, L.-Q. Chen, An inertial nonlinear energy sink, J. Sound Vib. 450 (2019) 199–213.
[38] A.H. Nayfeh, D.T. Mook, Nonlinear Oscillations, John Wiley & Sons, 2008.
[39] Z.N. Ahmadabadi, S. Khadem, Nonlinear vibration control and energy harvesting of a beam using a nonlinear energy sink and a piezoelectric device, J. Sound Vib. 333 (19) (2014) 4444–4457.
[40] Y.-H. Sun, Y.-W. Zhang, H. Ding, L.-Q. Chen, Nonlinear energy sink for a flywheel system vibration reduction, J. Sound Vib. 429 (2018) 305–324.
[41] L. Zuo, S.A. Nayfeh, The two-degree-of-freedom tuned-mass damper for suppression of single-mode vibration under random and harmonic excitation, J. Vib. Acoust. 128 (1) (2006) 56–65.
[42] Y. Liu, C.-C. Lin, J. Parker, L. Zuo, Exact H2 optimal tuning and experimental verification of energy-harvesting series electromagnetic tuned-mass dampers, J Vib Acoust 138 (6) (2016).